Modeling the Seasonal Cycle of the Upper Ocean

PHILIPPE GASPAR

Institut d'Astronomie et de Géophysique G. Lemaître, Université Catholique de Louvain, Belgium

(Manuscript received 2 September 1986, in final form 17 July 1987)

ABSTRACT

The parameterization of the turbulence used in one-dimensional oceanic mixed layer models is briefly reviewed, focusing on the long-term response of these models. Particular attention is directed towards the parameterization of turbulent dissipation. A general parameterized form is proposed that provides a useful guideline to devise new parameterizations and to compare existing ones. Different models of the classical Niiler–Kraus type are first tested by simulating four years (1969–72) of the upper ocean evolution at Ocean Station Papa. In the results, distinction is made between the errors inherent in the model and those due to changes in the upper ocean heat content not explained by the surface heat fluxes. It appears that, after a needed empirical calibration, all models systematically overestimate the sea surface temperature (SST) in summer and underestimate it during fall. In absolute value, the maximum error on the monthly-mean predicted SST reaches about 1 K. In an attempt to reduce this error, a new model, CMO, is presented. It includes a novel parameterization of the turbulent dissipation in which the rotation and stability effects are explicitly taken into account. Garwood's closure technique is used. The CMO is calibrated independently of the observations to be simulated. A four-year simulation at Station P shows that the error in the CMO-predicted SST reaches a maximum of only 0.5 K. However, the remaining error keeps an annual cycle similar to that observed with the other models. The obtained enhancement and the persistent error are analyzed.

1. Introduction

It has long been recognized that the ocean is a major component of the climate system. Limiting the study to time scales of a few years, the role of the deep ocean may be neglected and only the upper oceanic layers have to be considered. Their physics consist of (i) horizontal advection-diffusion processes linked to the ocean dynamics and (ii) thermodynamic processes and vertical turbulent mixing processes driven by the local surface fluxes of energy and water. The forcing by the surface fluxes dominates the advective effects over much of the world's oceans and is still of considerable importance (e.g., Schopf and Cane, 1983) in areas where the ocean dynamics play a leading part, namely, in the boundary regions and along the equator. The one-dimensional models of the upper ocean are, therefore, rather successful in simulating the evolution of the upper oceanic layers and, more particularly, the sea surface temperature (SST), a key factor in ocean–atmosphere interactions. For this reason, they are often considered as "first generation ocean models" (Elsberry and Garwood, 1980), thanks to which simple simulations of the interactive ocean–atmosphere system are feasible. They are also of great use as process models to include in more comprehensive models of the ocean or of the coupled ocean–atmosphere system.

Corresponding author address: Dr. Philippe Gaspar, Centre National de Recherches Météorologiques (DMN/EERM). 42 Avenue Coriolis, 31057 Toulouse Cedex, France.

The purpose of this work is to evaluate precisely the performance of these one-dimensional models for long-term simulations such as those needed for climate studies. This can be particularly useful when such a model is used as a component of a coupled ocean–atmosphere model. Indeed, in order to correctly interpret the results of a global model, it is very desirable to have a definite knowledge of the response of each of its component parts (Manabe et al., 1979).

Following the lead of Kraus and Turner (1967), so-called bulk models were first developed. They only predict the evolution of integral properties of the upper mixed layer (ML), assuming that the turbulence is efficient enough to mix uniformly all the physical properties within this layer. For the seasonal thermocline, use is made of a simple multilayer model. More sophisticated grid-point models were developed later (Mellor and Durbin, 1975). They use high-order turbulence closure schemes and therefore allow for a better understanding of the turbulent mechanisms that appear in the upper ocean. Furthermore, their results can be used to devise, and even calibrate, parameterizations of turbulence for use in simpler models. Nevertheless, the turbulence closure models are computationally much less efficient than the bulk models. The latter are thus generally preferred for long-term simulations and will accordingly receive our attention.

A large number of bulk models have already been proposed (see the review by Zilitinkevich et al., 1979) and most advances in this type of modeling have been synthesized in the now-classical model of Niiler and

Kraus (1977, hereafter referred to as NK). Most of the bulk models, however, were not specifically conceived for long-term simulations. In this paper, the equations basic to these models and the turbulence parameterizations used for their closure will be quickly reviewed, placing emphasis on the terms that govern the long-term response. Special attention will be directed towards the parameterization of the turbulent dissipation since it is an important but also weak point of the existing models (NK).

A few authors (Thompson, 1976; Martin, 1985) have tested bulk models on simulations of a single annual cycle using realistic forcing. The tests will be extended here over several years. In this way, it might be possible to determine if the simulation errors tend to grow or disappear from year to year, or if some errors systematically repeat at the same time of year. These tests will use data from the Ocean Weather Station P (50°N, 145°W) in the Northeast Pacific Ocean since the advective effects are known to be weak at this location. Furthermore, in addition to the typically recorded data, hourly measurements of the solar radiation are available at Station P. This is a component of the surface forcing that is particularly difficult to estimate accurately using parametric methods (Dobson et al., 1982).

Typical models of the NK type will be tested first and their errors analyzed. Emphasis will be placed on the SST simulation because of its particular importance for climate studies. Then, in an attempt to reduce the observed errors, a new model will be presented and tested.

2. Basic equations

On the assumption of vertical uniformity of temperature and salinity within the ML, the heat and salt conservation laws, integrated over the ML depth yield

$$h\frac{\partial T_m}{\partial t} = \overline{T'w'}(-h) - \overline{T'w'}(0) + \frac{F_{\text{sol}}}{\rho_0 c_p}[1 - I(-h)] - K_H\frac{\partial \bar{T}}{\partial z}(-h) \quad (1)$$

$$h\frac{\partial S_m}{\partial t} = \overline{S'w'}(-h) - \overline{S'w'}(0) - K_S\frac{\partial \bar{S}}{\partial z}(-h) \quad (2)$$

where a prime denotes a turbulent fluctuation and an overbar a Reynolds-average; h is the ML depth, T, S and w are the temperature, salinity and vertical velocity, T_m and S_m the depth-independent values of T and S within the ML, t the time, z the vertical coordinate, ρ_0 and c_p the reference density and specific heat of sea water, F_{sol} the absorbed solar irradiance, $I(z)$ the fraction of F_{sol} that penetrates to the depth z, K_H and K_S the diffusivities of heat and salinity below the ML.

The vertical turbulent fluxes at $z = -h$ are determined by the so-called jump equations whose general form is

$$-\overline{a'w'}(-h) = w_e\Delta a \quad (3)$$

where a stands for any physical variable, Δa denotes the discontinuity (jump) of a across the base of the ML and w_e is the entrainment velocity defined by

$$w_e = \partial h/\partial t, \quad \partial h/\partial t > 0$$

$$w_e = 0, \quad \partial h/\partial t \leq 0.$$

The surface fluxes are specified as follows:

$$-\rho_0 c_p\overline{T'w'}(0) = F_{\text{nsol}} \quad (4)$$

$$-\rho_0\overline{S'w'}(0) = (F_{w\uparrow} - F_{w\downarrow})S_m \quad (5)$$

where F_{nsol} is the "nonsolar" part of the surface heat flux, i.e., the net infrared flux plus the latent and sensible heat fluxes; $F_{w\downarrow}$ and $F_{w\uparrow}$ are the precipitation and evaporation rates. The evolution of temperature and salinity below the ML are given by

$$\frac{\partial \bar{T}}{\partial t} = \frac{F_{\text{sol}}}{\rho_0 c_p}\frac{\partial I}{\partial z} + \frac{\partial}{\partial z}\left[K_H\frac{\partial \bar{T}}{\partial z}\right] \quad (6)$$

$$\frac{\partial \bar{S}}{\partial t} = \frac{\partial}{\partial z}\left[K_S\frac{\partial \bar{S}}{\partial z}\right]. \quad (7)$$

To close the system, an equation governing the evolution of the ML depth h is required. Following the early lead of Ball (1960) and Kraus and Turner (1967), this equation is obtained from the turbulent kinetic energy (TKE) budget of the ML:

$$\frac{1}{2}\int_{-h}^{0}\frac{\partial \bar{E}}{\partial t}dz = \underbrace{\overline{\left(\frac{E}{2} + \frac{p'}{\rho_0}\right)w'}(-h)}_{\text{(I)}} - \underbrace{\overline{\left(\frac{E}{2} + \frac{p'}{\rho_0}\right)w'}(0)}_{\text{(II)}} - \underbrace{\int_{-h}^{0}\overline{\mathbf{U}'w'}\cdot(\partial\bar{\mathbf{U}}/\partial z)dz}_{\text{(III)}} + \underbrace{\int_{-h}^{0}\overline{b'w'}dz}_{\text{(IV)}} - \underbrace{h\epsilon_m}_{\text{(V)}} \quad (8)$$

where $\bar{E}/2$ is the TKE, $\mathbf{U} = (u, v)$ the horizontal velocity vector, p the pressure, ϵ_m the vertical mean over the ML of ϵ, the turbulent dissipation rate, and b the buoyancy defined by

$$b = g(\rho_0 - \rho)/\rho_0 \quad (9)$$

where g is gravity and ρ is given by the equation of state:

$$\rho = \rho_0[1 - \alpha(T - T_0) + \beta(S - S_0)] \quad (10)$$

with T_0 and S_0 the reference temperature and salinity and α and β the thermal expansion and saline contraction coefficients of sea water.

3. Parameterization of the TKE budget

For model closure, all the terms of (8) have to be expressed as functions of the inputs or variables of the model. Except for the dissipation term (VI), that will be treated in section 4, the parameterizations used are now classical (e.g., see NK). They will be briefly re-

viewed, having in mind our specific goal: the simulation of the long-term response of the ML.

1) Niiler and Kraus show that the flux of TKE at the base of the ML (II) is a generally negligible term. To resolve seasonal to diurnal variations, (I) may also be neglected (Garwood and Yun, 1979). This term only becomes important for shorter term variations (e.g., Gargett et al., 1979) but that is not of interest in this particular work.

2) Following Kraus and Turner (1967), the surface flux of TKE and pressure fluctuations (III), mainly caused by the surface breaking waves, is parameterized as follows:

$$-\overline{\left(\frac{E}{2}+\frac{p'}{\rho_0}\right)w'(0)} = m_2 u_*^3 \tag{11}$$

where m_2 is a constant to be determined and u_* the surface friction velocity. Notice that Kitaigorodskii et al. (1983) have shown that the flux of TKE generated by the surface breaking waves reaches values considerably larger than several times u_*^3. However, most of this energy is dissipated in the zone of wave influence, near the surface, so that the classical scaling of a constant stress layer applies just below that zone (Dillon et al., 1981; Oakey, 1985). Consequently, the relation (11) has to be interpreted as a bulk parameterization of the net surface flux of TKE (total flux minus dissipation in the zone of wave influence).

3) The TKE shear production term (IV) is parameterized in the form

$$\int_{-h}^{0} -\overline{\mathbf{U}'w'}\cdot(\partial\bar{\mathbf{U}}/\partial z)dz = m_3 u_*^3 \tag{12}$$

where m_3 is a constant. Numerical results from second-order (Klein, 1979) and third-order (Warn-Varnas et al., 1981) turbulence closure models show that, in the long-term, (12) provides a good estimation of the depth integrated shear production of TKE, regardless of the vertical distribution of the current within the ML. As suggested by Niiler (1975), several authors add to this basic parameterization the so-called Dynamic Instability Term (DIT = $0.5w_e(\Delta u^2 + \Delta v^2)$). This rapid transient term, with a response time one-half of an inertial period (Pollard et al., 1973) will be neglected here.

4) Using (9) and (10), a linear combination of the heat and salt equations yields the equation for buoyancy. Integrating it twice over z, one obtains (e.g., Kim, 1976)

$$\int_{-h}^{0} \overline{b'w'}dz = -0.5h\Delta b w_e - 0.5hB(h) \tag{13}$$

where

$$B(h) = -\overline{b'w'}(0) + \frac{\alpha g}{\rho_0 c_p}F_{sol}\left[1 + I(-h) - \frac{2}{h}\int_{-h}^{0} I(z)dz\right]. \tag{14}$$

Up to this point, the parameterized expression of the TKE budget of the ML amounts to

$$0.5h\Delta b w_e = (m_2 + m_3)u_*^3 - 0.5hB(h) - h\epsilon_m. \tag{15}$$

This basic formulation is common to most ML models. The differences arise essentially from the parameterization of the dissipation.

4. A unified approach to the parameterization of turbulent dissipation

a. General formulation for the dissipation

As shown by experimental studies (e.g., Willis and Deardorff, 1974), the dissipation is a dominant term in the TKE balance of a ML, and numerical studies reveal that the models are very sensitive to the chosen parameterization of this term (Niiler, 1977; Stevenson, 1979). However, this is still the most controversial and weakest point of the ML models (NK). Rather than examining the merits and faults of the several existing formulations, a unified approach is proposed. It is based on Kolmogorov's (1942) parameterization of the dissipation:

$$\epsilon = \bar{E}^{3/2}/l_\epsilon \tag{16}$$

where l_ϵ is a dissipation length linked to the size of the most energetic turbulent eddies. This expression can be appropriately extended for use in ML models under the form:

$$\epsilon_m = \sigma_e^3/l \tag{17}$$

where σ_e is a characteristic value of the turbulent velocity within the ML and l an integral dissipation length. The ML physics provide a list of characteristic length scales on which the dissipation length should depend (Resnyanskiy, 1975; Zeman and Tennekes, 1977, Garnich and Kitaigorodskii, 1977). Formally one may write:

$$l = F(h, L, \lambda, L_\Delta, L_N) \tag{18}$$

with

- F a function to be determined
- L $[=u_*^3/B(h)]$, a bulk Monin–Obukhov length
- λ $[=u_*/f]$, the Ekman length scale
- f the Coriolis parameter
- L_Δ $[=(\Delta u^2 + \Delta v^2)/\Delta b]$, a Monin–Obukhov length appropriate to the entrainment zone
- L_N $[=(\bar{E}^{1/2}/N)(-h)]$, a length characterizing the stratification at the bottom of the ML
- N the Brunt-Vaïsälä frequency.

It is clear from NK, that L_Δ is the relevant length scale for the dissipation of the TKE generated by the DIT. As this term is neglected here, L_Δ will also be omitted. Furthermore, the use of L_N in (18) seems to be appropriate only if Δb is relatively small (Zeman and Tennekes, 1977; Driedonks, 1982). Such a situation is often observed in the atmospheric boundary layer but is unusual in the ocean and recent works of oceanographic

interest (Kitaigorodskii, 1981; Deardorff, 1983) have purposely avoided the use of a stratification length scale for modeling the ML evolution. This lead will be followed here. Consequently, using dimensional analysis, (17) can be rewritten

$$h\epsilon_m = h\sigma_e^3/l = \sigma_e^3 G(h/L, h/\lambda) \tag{19}$$

where G is a dimensionless function of the Monin–Obukhov stability parameter, h/L and the Rossby rotation parameter, h/λ. Observations of the atmospheric boundary layer suggest that l decreases for increasing stability (Louis et al., 1983). It is also argued that rotation limits the vertical size of the eddies and hence l. Accordingly, we shall require that the ratio h/l, or equivalently G, is an increasing function of both the stability and the rotation parameters:

$$\frac{\partial G}{\partial(h/L)} \geqslant 0 \tag{20a}$$

$$\frac{\partial G}{\partial(h/\lambda)} \geqslant 0. \tag{20b}$$

Similar constraints are applied in the atmospheric boundary layer model of Therry and Lacarrère (1983).

b. Analysis of existing parameterizations

Most parameterizations of dissipation used in ML models are consistent with (19) if one assumes that

$$\sigma_e = u_*. \tag{21}$$

In this case, (19) reduces to the general expression proposed by Resnyanskiy (1975). The commonly applied parameterization of NK simply assumes that a constant fraction of each production term is dissipated, i.e.,

$$h\epsilon_m = m_d u_*^3 + 0.25(1 - n)h[|B(h)| - B(h)] \tag{22}$$

with $0 \leqslant m_d \leqslant m_2 + m_3$ and $0 \leqslant n \leqslant 1$. Dividing (22) by u_*^3, we obtain the expression of h/l implicitly used by NK:

$$h/l = m_d + 0.25(1 - n)[|h/L| - h/L].$$

No dependence on h/λ appears in this relation. The ratio h/l remains constant in stable cases ($h/L > 0$) but, contrary to what was expected [cf. (20a)], it is a decreasing function of h/L in unstable situations. Approaching the pure convection regime ($h/L \to -\infty$), h/l tends to become infinite. The origin of this paradox has to be found in the chosen definition of σ_e (21). Indeed, in convective situations, u_* is not an adequate turbulent velocity scale. It underestimates the real turbulent velocity so that a spurious increase of h/l is necessary to maintain the dissipation at its correct level. This remark essentially brings to light that a rather artificial behavior of h/l is imposed when u_* is chosen as the characteristic turbulent velocity scale. In this case, it is impossible to control explicitly the dependence of h/l on the stability parameter.

On the other hand, when (22) is used, a constant fraction of the TKE production is used for entrainment independently of the ML depth. Several authors have pointed out that this formulation invariably leads to an overestimation of the entrainment velocity w_e in deep MLs. As a consequence, a repeatable annual cycle cannot be simulated. To guard against this shortcoming, Alexander and Kim (1976), Elsberry et al. (1976) and Niiler (1977) proposed some rather artificial ad hoc parameterizations of the dissipation. Based on the observation that, in neutral and stable situations, a turbulent boundary layer reaches a maximum depth proportional to h/λ, other authors devised expressions in which the fraction of dissipated TKE grows with h/λ, in accordance with (20b). For this purpose, the constant m_d in (22) is generally replaced by an increasing function of h/λ. A simple linear growth yields (Resnyanskiy, 1975):

$$h\epsilon_m = (ch/\lambda)u_*^3 + 0.25(1 - n)h[|B(h)| - B(h)] \tag{23}$$

where c is a positive constant. Wells (1979) rather proposes an exponential formulation:

$$h\epsilon_m = (m_2 + m_3)[1 - \exp(-h/\lambda)]u_*^3 + 0.25(1 - n)h[|B(h)| - B(h)]. \tag{24}$$

The merits of (22), (23) and (24) will be compared in annual simulations of the ML. The NK formulation will be first calibrated and tested.

5. Calibration of the NK model

Using (22) the equation for h (15) reduces to

$$h\Delta b w_e = 2mu_*^3 - 0.5h[(1 - n)|B(h)| + (1 + n)B(h)] \tag{25a}$$

where $m = m_2 + m_3 - m_d$. When the ML is shallowing, the left-hand side of (25a) becomes zero and h is determined from the resulting algebraic relation:

$$h = 2 \text{ mL}. \tag{25b}$$

Numerous articles deal with the identification of the two constants m and n. The value of n can be deduced from observations of convective flows ($u_* = 0$, $B(h) < 0$). Detailed observations of such flows in the ocean are few (Farmer, 1975; Shay and Gregg, 1984). Therefore, information originates mainly from laboratory experiments and observations of convective atmospheric boundary layer. Some important review papers and recent observational results concerning the value of n are listed in Table 1. They all are in close agreement and sustain the choice:

$$n = 0.2. \tag{26}$$

The value of m can be obtained from observations of neutral shear flows ($u_* > 0$, $B(h) = 0$). Several experiments on such flows were performed in annular tanks

TABLE 1. Some published values of the constant n appearing in Eq. (25a).

Author	n	Source
Stull (1976)	0.1 . . . 0.3	Review of published values
Heidt (1977)	0.18	Review of published values and laboratory experiments
Artaz and André (1980)	0.2	Review of published values and numerical experiments with the André et al. (1978) model
Driedonks (1982)	0.2	Observations of the atmospheric boundary layer from a meteorological mast
Boers et al. (1984)	0.22	LIDAR observations of the atmospheric boundary layer

(for a review see Deardorff and Yoon, 1984). However, Scranton and Lindberg (1983) demonstrated that the entrainment rates measured in these experiments depend on annulus curvature and geometry. Consequently, these data should not be directly applied to oceanic studies. On the other hand, the estimates of m deduced from oceanic observations are largely scattered (see Gargett et al., 1979), and it is extremely difficult to compare the different published values because of the disparity of the techniques used to identify m. Yet the results from the MILE experiment have to be singled out. During this large cooperative experiment, intensive measurements of the upper ocean took place over a continuous 20-day period (Davis et al., 1981a). After detailed analysis of these data and elimination of the surface buoyancy flux effects, Davis et al. (1981b) found:

$$0.4 \leqslant m \leqslant 0.5. \tag{27}$$

This is probably the best estimate of m available at present.

6. Model testing at *Weathership P*

a. *Numerical characteristics*

The equations of the models are set up for a finite-difference solution. In all the simulations, a time step of 3 h was used. The vertical discretization grid had a uniform resolution of 2 m from the surface to a depth of 150 m. The ML depth is not forced to coincide with the depth of a discretization level and, when the ML retreats, the density profile is adjusted following the Adamec et al. (1981) algorithm so as to conserve potential energy. The parameters α and β are allowed to vary as a function of the ML temperature and salinity. They are computed following Bryan and Cox (1972). To begin with, K_H and K_S were assumed to be equal to zero. The very small value of $K_H = 2 \times 10^{-6}$ m^2 s^{-1}, used by Martin (1985) for simulations at Station P, is not significantly different from this first choice.

b. *Initialization*

Bathythermograph observations, usually made every three hours at Station P, are directly used to initialize the temperature profile. Data concerning the salinity profile are much sparser. Yet model experiments (Martin, 1985) have shown that the surface salinity fluxes at Station P can only have a small effect on the vertical mixing. These fluxes are therefore neglected here and a time-independent climatological salinity profile (Tabata, 1964) is used. From the surface to a depth of 110 m the salinity keeps a constant value of 32.8‰. Below 110 m, the salinity increases linearly and reaches 33.7‰ at 150 m. This strong halocline is maintained throughout the year. It strongly reduces the entrainment as soon as the ML depth reaches the halocline depth at the beginning of each winter.

c. *Surface forcing*

The first meteorological observations at Station P were taken in 1949. The station was closed in 1981. Data for the 1960s and 1970s were investigated and a period of almost four years (0900 UTC 1 January 1969 to 0900 UTC 25 December 1972) was selected for its excellent data coverage. Only 0.3% of the three-hourly synoptic observations and 6.8% of the hourly measurements of the incoming solar radiation are missing. From the available measurements of radiation, air and wet-bulb temperature, SST (bucket temperature), wind speed and cloudiness, Tricot (1985) (henceforth TR) estimated the three-hourly values of the surface forcing (u_*, F_{sol}, F_{nsol}) used in our simulations. For the sake of completeness, the principal characteristics of the data treatment performed by TR are given here.

The wind speed is first corrected to 10 m height using the algorithm of Kondo (1975) using Wu's (1982) drag coefficient. The same drag coefficient is then used to compute u_*. Most values of the surface incoming solar radiation are directly obtained from the observations. The missing ones are estimated using the Smith and Dobson (1984) formula. The sea surface albedo is taken from Payne (1972). The sea water at Station P is of the Jerlov's (1976) optical type II. The absorption law for the solar irradiance $I(z)$ is parameterized following Paulson and Simpson (1977). The infrared flux is obtained from an adapted version of the Lind and Katsaros (1982) model. The latent and sensible heat fluxes are calculated with the Friehe and Schmitt (1976) bulk aerodynamic formulae.

d. *Analysis of the heat budget*

After calibration of the rough BT data, using the bucket SST as a reference, three-day mean values of the heat content of the upper 125 meters were computed. The observed changes (OC) of that heat content are plotted on Fig. 1 and compared to the changes due to the surface heat fluxes (SC). The value of SC was

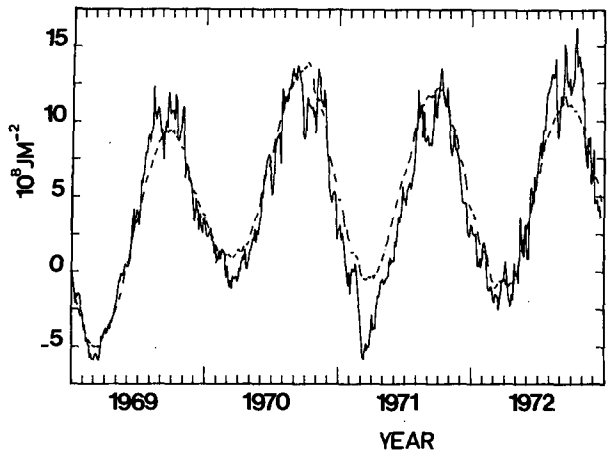

FIG. 1. Variations of the upper layers (0–125 m) heat content at Station P (1969–72) deduced from 3-day mean BT data (OC; solid curve) and variations accounted for by the surface fluxes (SC; dashed curve).

calculated using the TR fluxes integrated over successive periods of 3 days. The figure shows that, during this 4-year period, the heat budget is closed using the surface fluxes only. The seasonal and interannual changes of the heat content are well accounted for by the surface fluxes. The shorter-term variability of OC is mainly due to up and down displacements of the isotherms within the thermocline. This effect is particularly important each year between July and October, when a strong seasonal thermocline occupies most of the considered layer. It is mainly responsible for the large differences that appear each summer between OC and SC. Gaspar (1985b) indeed observed that, above the summer thermocline between 0 and 60 m, the heat content changes are well correlated with the surface fluxes while, below, they are principally related to the vertical oscillations of the thermocline. A similar behavior was remarked in the equatorial Indian Ocean by McPhaden (1982) who pointed out that, the vertical motions of the thermocline may have little or no effect on the SST variability.

This behavior, however, cannot provide an explanation for the large difference (up to 4 10^8 J m^{-2}) between OC and SC that existed in March and, to a lesser extent, April 1971. Indeed, during this period of the year, the seasonal thermocline is reduced to zero and the ML reaches a depth between 100 and 120 m. The BT profiles reveal that the temperature of the water column between 0 and 125 m decreased by 0.8 K during the final week of February. This massive cooling cannot be accounted for by the surface heat fluxes. Nor can these explain the strong warming observed in April that almost restored the agreement between OC and SC. These successive cooling and warming are most probably of advective origin but no specific study of these events has been performed. It suffices here to observe that the surface heat fluxes do account for the seasonal changes in heat content, except for March and April 1971. During these months, the temperature simulated by any one-dimensional model forced with these fluxes should be up to 0.8 K above the observations.

Annual mean values of the TR surface forcing are given in Table 2. The 4-year mean values of the surface heat fluxes are as follows: F_{sol} = 101 W m^{-2}, latent plus sensible flux = −57 W m^{-2}, net infrared flux = −40 W m^{-2}; total = 4 W m^{-2}. For a 17-year mean, Smith and Dobson (1984) found a total heat gain at Station P of 32 W m^{-2}, while the same authors using Bunker's (1976) formulae obtained a heat loss of 23 W m^{-2}. The TR intermediate value, corroborated by the observed changes in heat content, is comparable with the small heat gain of 3.4 W m^{-2} computed by Martin (1985) for the period 1960–70.

e. *Simulations with the NK model*

The NK model was first integrated for the year 1969. This simulation immediately showed that, for the chosen values of the parameters m and n, the model predicted SST was too high. The difference between the simulated and observed monthly mean SST (ΔSST) reached more than 3 K during August and September. This error is due to a systematic underestimation of the ML depth resulting in an excessive warming of the summer ML. This underestimation of the ML depth is revealed by the comparison of Fig. 2a, b. Yet, some care has to be taken when comparing the observed and simulated values of h. The observed value of h is taken here as the depth of the first maximum in the BT temperature gradient. The resolution of the BT data, however, is rarely sufficient to detect small transient thermoclines. These are therefore generally overlooked and the graph of the so-called observed values of h represents, in fact, the lower envelope of the real ML depths (Woods, 1983). Nevertheless, even the lower envelope of the simulated ML depths is clearly above the observed ML depths. Notice also that, from January to March, the ML depth plotted on Fig. 2a is larger than the depth of the halocline. Consequently, it is not representative of the real ML depth which should then be determined from salinity profiles.

In order to simulate more realistic (deeper) MLs, one can increase the wind-mixing efficiency. Several annual runs were performed with progressively higher

TABLE 2. Annual mean values of the TR surface forcing.

Year	Wind speed at 10 m (m s^{-1})	Solar irradiance (W m^{-2})	"Nonsolar" heat flux (W m^{-2})	Net heat flux (W m^{-2})
1969	9.6	99.0	−87.0	12.0
1970	9.6	96.0	−92.0	4.0
1971	10.3	103.0	−105.0	−2.0
1972	9.1	106.0	−104.0	2.0

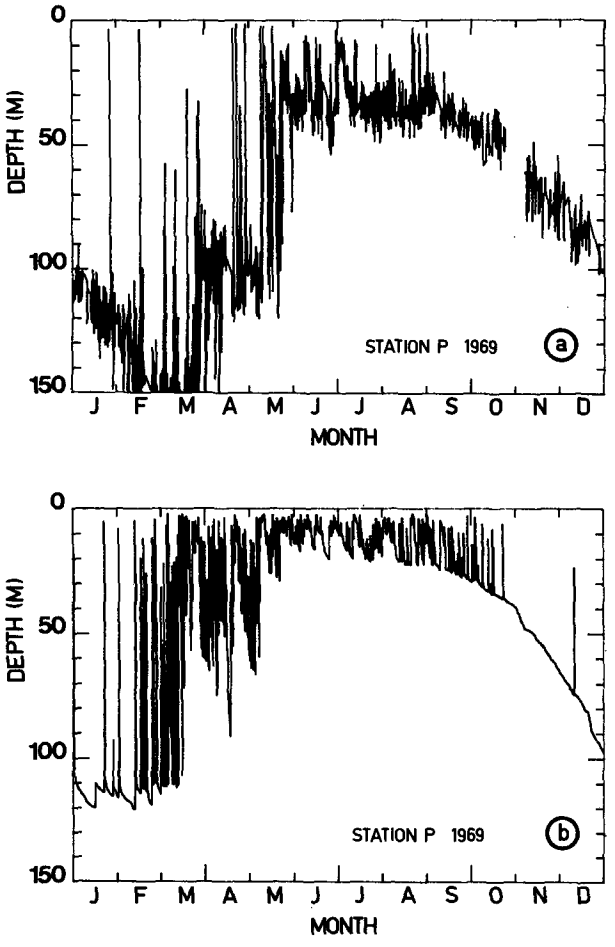

FIG. 2. Three-hourly ML depth at Station P during the year 1969. (a) Observation. (b) Simulation by the NK model with $m = 0.45$ and $n = 0.2$.

values of m. As seen on Figure 3a, the increase of m considerably reduces the overestimation of the summer SST but induces an underestimation of the temperature in autumn. This excessive autumn cooling is due to a too rapid erosion of the summer thermocline (compare Figs. 2a and 3b during autumn).

The model was next tested with a four-year simulation, using $m = 0.65$, the value that minimizes the maximum of ΔSST in 1969. In this simulation, the foreseen SST overestimation of March 1971 is evident (Fig. 4) but another important discrepancy appears in September of the same year (ΔSST = 1.2 K). This large error is triggered by a storm reaching its maximum intensity (wind speeds up to 20 m s^{-1}) on 11 September, when the ML is still quite shallow (h between 30 and 40 m). A preliminary analysis of the results led the author (Gaspar, 1985a) to postulate that the model's shortcoming was due to the omission of the DIT, leading to an insufficient deepening, and hence an insufficient cooling, of the ML during this storm. A more comprehensive study shows that the model's response to several other storms is quite correct, though a bit slow, as could be expected. So, it does not seem that the omission of the DIT is susceptible to produce an error the size of that observed in September 1971. On the other hand, an analysis of the BT data around 11 September reveals a peculiar event. At the beginning of the wind event, the ML is actively entraining and a very strong thermal stratification exists just below it with temperature gradients reaching 1 K m^{-1}. Then rapidly, this stratification is modified and the previously concentrated temperature gradient spreads throughout the whole thermocline, indicating that some very effective mixing has reached the thermocline itself. Such a behavior cannot be simulated by our simplistic thermocline model. Consequently, the simulated temperature gradient below the ML remains too large, slows down the deepening and causes an overestimation of the SST. This vanishes only when the seasonal thermocline has been almost completely eroded by the end of December. The thermocline dynamics during this

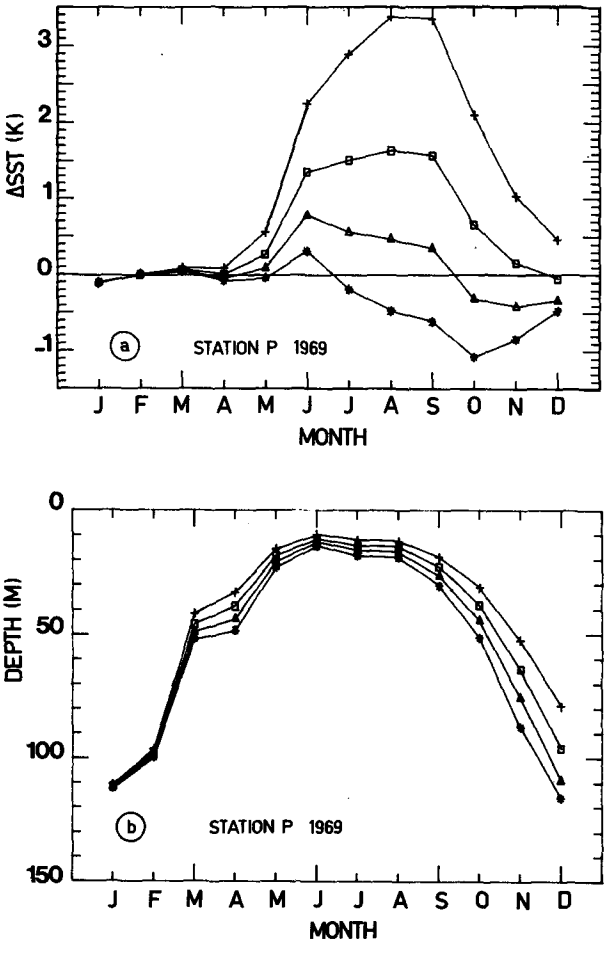

FIG. 3. (a) Difference between the simulated and observed monthly mean SST(ΔSST) and (b) monthly mean value of the simulated ML depth for the NK model with successively $m = 0.45$ (+), $m = 0.55$ (□), $m = 0.65$ (△) and $m = 0.75$ (*). Station P, year 1969.

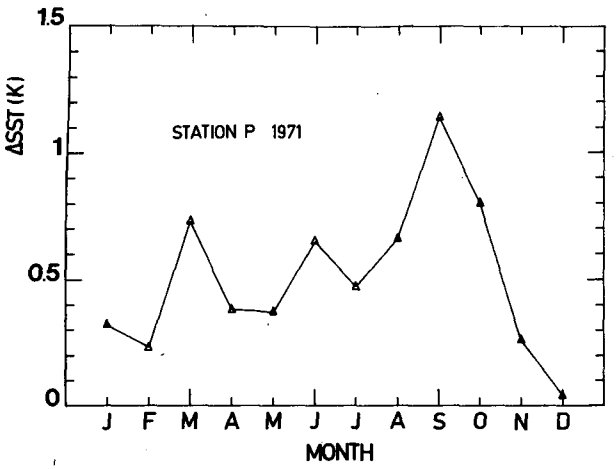

FIG. 4. ΔSST for the NK model with $m = 0.65$. Station P, year 1971.

event certainly deserve further studies but this is beyond the scope of this work. For the purpose of testing ML models, we will consider that 1971 is mostly an anomalous year.

For the three other years, Fig. 5 shows that the error in the simulated SST has a characteristic annual cycle: the SST is systematically overestimated in summer and underestimated in autumn. This is associated with an underestimation of the summer ML depth and a too rapid autumnal erosion of the thermocline. The error on the SST has noticeable interannual variations but it typically oscillates between −1 K and 1 K. Some additional 4-year simulations were carried out with slightly increased or decreased values of m. As a general rule, an increase of m reduces the summer SST error but increases the autumn error. The opposite is observed when reducing m. The best choice for m varies a little from year to year. Globally, the best results were obtained for

$$0.55 \leqslant m \leqslant 0.7. \tag{28}$$

In ML simulations over the Northern Hemisphere oceans, Miyakoda and Rosati (1984) also obtained an insufficient mixing and excessive SST during the summer months. This error appeared with both a NK and a Mellor and Durbin (1975) model. There are some indications of the same problem in the Martin (1985) numerical experiments. Martin (1985) showed that the accuracy of the NK model is enhanced when the value of m used for deepening (in 25a) is smaller than that used for shallowing (in 25b). With such an ad hoc modification, one indeed counters the excessive summer shallowing and slows down the autumn entrainment, as needed.

The sensitivity of the model to the diffusion of heat within the thermocline was also tested. The estimate of the heat diffusivity K_H is largely uncertain (e.g., Garrett, 1979) but numerical simulations show (Gaspar, 1985b) that, whatever the value of K_H is, the SST is almost unaffected by heat diffusion between January and May, as the thermocline stratification is weak throughout this period. The downward diffusive flux of heat becomes important in June but the maximum resulting decrease of the SST (relative to the case with $K_H = 0$) is obtained only in September–October. This means that the simulation of the heat diffusion below the ML mainly reinforces the already existing underestimation of the autumn SST while it only slightly reduces the overestimation of the summer SST. Consequently, the introduction of heat diffusion cannot correct for the systematic error of the NK model. It only adds an unknown (K_H) to the model without improving the SST prediction.

f. Simulations with the Resnyanskiy (1975) and Wells (1979) models

Introducing successively (23) and (24) into the TKE budget of the ML (15), the equation for h takes the form:

$$h\Delta bw_e = 2(m_r - ch/\lambda)u_*^3 - 0.5h[(1 - n)|B(h)| + (1 + n)B(h)] \tag{29}$$

with $m_r = m_2 + m_3$, for the Resnyanskiy model and

$$h\Delta bw_e = 2m_w \exp(-h/\lambda)u_*^3 - 0.5h[(1 - n)|B(h)| + (1 + n)B(h)] \tag{30}$$

with $m_w = m_2 + m_3$, for the Wells model.

Both expressions were tested on 4-year simulations. After some calibration experiments with the Wells model, the value $m_w = 0.8$ was chosen. For this choice, the accuracy of the SST prediction is almost identical to that of the NK model in summer (Fig. 5) but the autumn error is decreased by 0.3 to 0.4 K. The Res-

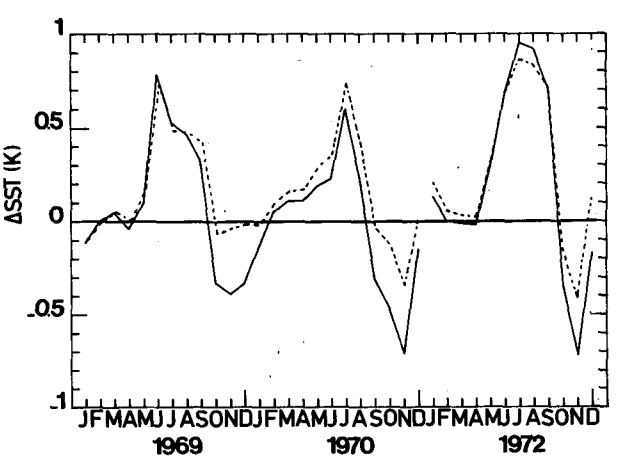

FIG. 5. ΔSST for the NK model ($m = 0.65$; solid curve) and for the Wells model ($m_w = 0.8$; dashed curve). Station P, years 1969, 1970 and 1972.

nyanskiy model leads to similar results with, for example, $m_r = 0.8$ and $c = 0.65$. The calibration of this model, however, is more problematical as it requires the tuning of two constants (m_r and c) instead of a single one for NK (m) or Wells (m_w).

To conclude, the results of the Resnyanskiy and Wells models indicate that the use of a rotation-dependent turbulent dissipation effectively reduces, but does not suppress, the autumn error. The systematic overestimation of the summer SST persists with the same magnitude and the models still require an empirical calibration. In an attempt to cope with these problems, a new model is presented in the next section.

7. A new model for the prediction of the ML depth

a. *Parameterization of turbulent dissipation*

Numerous observations of the atmospheric boundary layer (e.g., Caughey, 1982) and oceanic ML (e.g., Moum and Caldwell, 1985) demonstrate that the stability, as quantified by the Monin–Obukhov parameter, greatly influences the ML behavior. Starting from the general relation (19), it was observed in section 4b, that the stability-dependence of the dissipation length is difficult to specify as long as u_* is chosen as the characteristic turbulent velocity scale. Actually, in the framework of a bulk model, the best possible choice for σ_e is

$$\sigma_e{}^2 = E_m = \frac{1}{h}\int_{-h}^{0} \bar{E}dz. \tag{31}$$

This indeed yields the natural extension of the Kolmogorov relation (16) for depth-integrated models. It was first proposed by Garwood (1977, hereafter referred to as GAR) who also introduced the bulk closure technique needed to determine E_m, a supplementary model unknown. For the dissipation length GAR uses

$$h/l = k_1 + k_2(hf/E_m{}^{1/2}) \tag{32}$$

where k_1 and k_2 are positive constants. This relation does not call upon a stability dependence. Furthermore, GAR chooses $E_m{}^{1/2}/f$ as the characteristic rotational length scale but, as pointed out by Deardorff (1983), the physical mechanism behind that assumption remains unclear. Here, it is rather proposed to use a definition of h/l consistent with (19) and (20a, b). Since h/l is positive, in order to satisfy (20a) G must asymptotically reach its (positive) minimal value in the case of pure convection. In the absence of rotational constraint a simple function that meets this requirement is

$$G(h/L, 0) = a_1 + a_2 \exp(h/L) \tag{33}$$

where a_1 and a_2 are positive constants. Concerning the rotational constraint it is assumed that, when the ML depth exceeds the neutral height scale (0.4λ), this height becomes the main dissipation length instead of h. However, it does not seem that this constraint acts on convective turbulence (Deardorff, 1983; Therry and Lacarrère, 1983). Consequently, (33) is modified in the following way:

$$h/l = G(h/L, h/\lambda) = a_1 + a_2 \max[1, h/(0.4\lambda)] \exp(h/L). \tag{34}$$

The first equation for the prediction of h in the new model (hereafter called CMO) is simply the TKE budget (15) in which the dissipation is parameterized using (19), (31) and (34):

$$0.5h\Delta b w_e = (m_2 + m_3)u_*^3 - 0.5hB(h) - (h/l)E_m{}^{3/2}. \tag{35}$$

b. *The entrainment equation*

Oceanographers generally use a vertically integrated TKE budget to close their ML models, while atmospheric physicists rather employ the turbulent energy budget at the entrainment interface (e.g., see Zeman and Tennekes, 1977). Assuming the stationarity of the TKE, this budget reads:

$$-\overline{b'w'}(-h) = \underset{(P)}{-} \underbrace{\frac{\partial}{\partial z}\left[\overline{\left(\frac{E}{2} + \frac{p'}{\rho_0}\right)w'}\right](-h)}_{(T)} - \underbrace{[\overline{\mathbf{U}'w'} \cdot (\partial \bar{\mathbf{U}}/\partial z)](-h)}_{(M)} - \underbrace{\epsilon(-h)}_{(D)}. \tag{36}$$

The convergence of the TKE flux (T) and the local shear-production of turbulence (M) both provide energy for mixing at the bottom of the ML. A thorough knowledge on the behavior of these two source terms is thus fundamental for entrainment modeling. Garwood hypothesizes that (T) is the main source of energy for entrainment. He, therefore, assumes that (36) can be reduced to the definition of a critical parameter:

$$P_g = -\overline{b'w'}(-h) \Big/ \frac{-\partial}{\partial z}\left[\overline{\left(\frac{E}{2} + \frac{p'}{\rho_0}\right)w'}\right](-h). \tag{37}$$

On the contrary, in the widely quoted Mellor and Durbin (1975) model, (T) is assumed to be negligible throughout the ML. More generally, the same hypothesis is used in all low-order turbulence closure models. In these models, the turbulence, and hence the mixing, is essentially governed by the flux Richardson number:

$$R_f = -\overline{b'w'}/[-\overline{\mathbf{U}'w'} \cdot \partial \bar{\mathbf{U}}/\partial z].$$

Garwood indicated that, when writing his paper, experimental data failed to discriminate in favor of one of these two fundamentally different approaches. This still holds true. However, we have now at our disposal several turbulence closure models of the oceanic ML through which the TKE budget at the entrainment interface can be investigated. Mellor and Durbin (1975) first presented a "degenerated" second-order closure model, followed by second-order (Kundu, 1980a; Klein

and Coantic, 1981) and third-order (André and Lacarrère, 1985) turbulence closure models. They will hereafter be referred to as MD, KU, KC and AL, respectively. An analysis of their results shows:

(i) As in the integrated TKE budget (15), the TKE stationarity hypothesis used to obtain (36) is legitimate for simulations of the long-term response.

(ii) The MD model, that neglects the transport term (T), can be considered as a proof by contradiction that this term is important in the case of stress-driven entrainment. Indeed, this model needs to exaggerate the amount of TKE available for entrainment in order to predict a realistic deepening rate; MD obtain these large quantities of available TKE both by underestimating the dissipation, as noticed by Warn-Varnas and Piacsek (1979) and by overestimating the drag coefficient as remarked by Gargett et al. (1979) and Klein (1980); KC have clearly shown that the insufficient entrainment rate obtained by MD is mainly due to the absence of the transport term in their model. On the contrary, the KU model does not show a significant participation of (T) to the entrainment. However, this result is questionable as discussed by Deardorff (1980) and Kundu (1980b).

When the ML tends toward a convective regime, the vertical transport of TKE becomes more and more important for the ML dynamics, in general, and for entrainment in particular (e.g., AL). In the asymptotic case of pure convection (M) vanishes and (T) is the unique source of energy for entrainment. In summation, (T) is always an important term for entrainment and particularly large in convective situations.

(iii) KU, KC and AL all point out in their stress-driven experiments that the TKE generated by the shear of the current, when present at the base of the ML, contributes significantly to entrainment. However, AL show that, in the neutral case, the shear-generated turbulence is not sufficient to mix perfectly the momentum introduced at the surface by the wind stress. The resulting momentum distribution is characterized by an almost constant shear throughout the whole ML (the ML itself remains slightly stratified). However, as soon as some convection appears, the momentum tends to diffuse downward more easily, homogenizing the velocity profile within the ML and constraining the current shear to concentrate near the entrainment interface. The so enhanced shear generates TKE (M) which is then directly available for entrainment. The results of KC also show some evidence of such a behavior. This effect simulated by numerical models has recently been observed in the ocean by Price et al. (1986). In summation, (M) is an important term for entrainment. Its magnitude depends on the downward mixing of momentum that is enhanced by the convective activity.

From (ii) and (iii) one concludes that (T) and (M) are both important terms for entrainment. Consequently, instead of P_g or R_f, it is proposed to use the following critical parameter:

$$P_c = \frac{-\overline{b'w'}(-h)}{-\frac{\partial}{\partial z}\left[\overline{\left(\frac{E}{2}+\frac{p'}{\rho_0}\right)w'}\right](-h) - [\overline{\mathbf{U}'w'}\cdot(\partial\bar{\mathbf{U}}/\partial z)](-h)}. \quad (38)$$

Furthermore, it appears that the magnitude of the two source terms is dependent on the efficiency of a vertical turbulent transfer, of TKE for (T), and of momentum for (M). The characteristic time scale associated with this transfer is:

$$\tau = h/\sigma_w \quad (39)$$

where σ_w is a characteristic value of the vertical turbulent velocity. This second turbulent velocity scale, different from σ_e, is introduced because one needs a velocity that is truly representative of the vertical eddy transfer. The total rate of supply of TKE at the bottom of the ML, (T) + (M), can then be parameterized according to

$$-\frac{\partial}{\partial z}\left[\overline{\left(\frac{E}{2}+\frac{p'}{\rho_0}\right)w'}\right](-h) - [\overline{\mathbf{U}'w'}\cdot\partial\bar{\mathbf{U}}/\partial z](-h) = m_1'\sigma_e^2/\tau. \quad (40)$$

The introduction of (3), (39) and (40) into (38) yields the general entrainment equation

$$h\Delta b w_e = m_1\sigma_e^2\sigma_w \quad (41)$$

where $m_1 = m_1' P_c$. The characteristic turbulent velocity σ_e being defined by (31), a consistent choice for σ_w is

$$\sigma_w^2 = W_m = \frac{1}{h}\int_{-h}^{0}\overline{w'^2}dz. \quad (42)$$

Notice that the vertical component of the TKE, $\overline{w'^2}$, is very sensitive to the convective activity as the turbulent buoyancy flux directly feeds it. Finally, introducing (31) and (42) into (41), one obtains

$$h\Delta b w_e = m_1 E_m W_m^{1/2}. \quad (43)$$

This entrainment equation is identical to that of GAR though the reasoning leading to it is essentially different. To set up (43) we invoke a vertical turbulent transfer mechanism affecting both the TKE and the momentum throughout the ML. On the contrary, GAR bases his deduction on a study of the dynamical instability at the entrainment interface.

c. *The equation for W_m*

The equation for W_m is obtained from the vertically integrated equation for $\overline{w_2'}$:

$$\frac{1}{2}\int_{-h}^{0}\frac{\partial\overline{w'^2}}{\partial t}\,dz = \overline{\left(\frac{w'^2}{2}+\frac{p'}{\rho_0}\right)w'}(-h) - \overline{\left(\frac{w'^2}{2}+\frac{p'}{\rho_0}\right)w'}(0)$$

(I') (II') (III')

$$+\int_{-h}^{0}\overline{b'w'}dz + 2\Omega\cos\phi\int_{-h}^{0}\overline{u'w'}dz$$

(IV') (V')

$$+\frac{1}{2}\int_{-h}^{0}R_{33}dz - \int_{-h}^{0}\nu\overline{\frac{\partial w'}{\partial x_j}\frac{\partial w'}{\partial x_j}}\,dz \quad (44)$$

(VI') (VII')

where Ω is the angular speed of rotation of the earth, ϕ is the latitude, ν is the sea water molecular viscosity and R_{ij} is the pressure–strain correlation:

$$R_{ij} = \overline{\frac{p'}{\rho_0}\left(\frac{\partial v_i'}{\partial x_j}+\frac{\partial v_j'}{\partial x_i}\right)}$$

For the same reasons we neglected (I) and (II) in (8), the corresponding terms (I') and (II') will be omitted. The surface flux (III') is only a fraction of (III) in (8). It could also be taken proportional to u_*^3 but there is no information available to determine the constant of proportionality. Rather than including an unknown constant in the model, we prefer to neglect this term, as done by GAR. The buoyancy term (IV') has already been integrated [Eq. (13)]. The Coriolis term (V') is generally small and is neglected in most turbulence closure models. This will also be done here though some recent works of Garwood et al. (1985) indicate that this term can, in some circumstances, be important. Assuming that the dissipation is isotropic within the dissipation subrange, one takes

$$\int_{-h}^{0}\nu\overline{\frac{\partial w'\partial w'}{\partial x_j\partial x_j}}\,dz = \frac{h}{3l}E_m^{3/2}. \quad (45)$$

The commonly accepted minimal parameterization of R_{ij} reduces to the return-to-isotropy term of Rotta (1951). However, it has been shown that this term only partially reproduces the effect of the pressure–strain correlation (e.g., Lumley and Khajeh-Nouri, 1974). Extended parameterizations have thus been proposed. From a review of these, Klein (1979) concludes that, for practical purposes, the Launder (1975) expression is most satisfying. For R_{33} it reads

$$\frac{1}{2}R_{33} = m_4\frac{\epsilon}{\bar{E}}\left(\frac{\bar{E}}{3}-\overline{w'^2}\right) + \frac{m_5}{3}\left[-\overline{\mathbf{U}'w'}\cdot(\partial\bar{\mathbf{U}}/\partial z) - 2\overline{b'w'}\right]. \quad (46)$$

Following the GAR technique, this relation is extended to the depth-integrated variables:

$$\frac{1}{2}\int_{-h}^{0}R_{33}dz = m_4\frac{h}{l}E_m^{1/2}\left(\frac{E_m}{3}-W_m\right) + \frac{m_5}{3}\left[-\int_{-h}^{0}\overline{\mathbf{U}'w'}\cdot(\partial\bar{\mathbf{U}}/\partial z)dz - 2\int_{-h}^{0}\overline{b'w'}dz\right]. \quad (47)$$

The two integrals in the last term are determined by (12) and (13). Furthermore, one assumes that the rotational constraint does not act upon the pressure-strain correlation. Accordingly, the characteristic length l is replaced in (47) by a similarly defined length l_p in which the rotational constraint is omitted, i.e.,

$$h/l_p = a_1 + a_2\exp(h/L). \quad (48)$$

Finally, all the proposed parameterizations being included into (44), the equation for W_m becomes

$$\left(\frac{1}{2}-\frac{m_5}{3}\right)[h\Delta bw_e + hB(h)] = \left(\frac{m_4h}{3l_p}-\frac{h}{3l}\right)E_m^{3/2} + \frac{m_5m_3}{3}u_*^3 - \frac{m_4h}{l_p}E_m^{1/2}W_m. \quad (49)$$

8. Characteristics of CMO

a. Implementation

The CMO set of equations (35), (43) and (49) includes seven constants (m_1 to m_5, a_1 and a_2) and governs the evolution of h, E_m and W_m. The constants can be determined using the results of several experiments on turbulent flows and one numerical result from the André and Lacarrère (1985) third-order turbulence closure model. This calibration is detailed in appendix A. The CMO has been primarily devised to predict the evolution of h. The determination of E_m and W_m is an auxiliary task that can be avoided by a method of solution developed in appendix B. It is shown there that the entrainment velocity is given by the following single equation:

$$h\Delta bw_e = \frac{-(0.5A_p + c_{p1}S_p) + [(0.5A_p - c_{p1}S_p)^2 + 2c_4(h/l)^2A_pS_p]^{1/2}}{c_4(h/l)^2 - c_{p1}} \quad (50)$$

where

$$A_p = c_{p3}u_*^3 - c_{p1}hB(h)$$

$$S_p = (m_2+m_3)u_*^3 - 0.5hB(h)$$

$$c_{p1} = [(2-2m_5)(l_p/l)+m_4]/6$$

$$c_{p3} = [m_4(m_2+m_3) - (l_p/l)(m_2+m_3-m_5m_3)]/3$$

$$c_4 = 2m_4m_1^{-2}.$$

The physical origin of the component terms in (50) are given in appendix B. It is also shown that the condition for entrainment ($w_e > 0$) reduces to

$$A_p > 0 \tag{51}$$

and that the retreat depth is obtained from the algebraic equation

$$A_p = 0. \tag{52}$$

Formally, (50) and (52) are similar to the corresponding entrainment and retreat equations of the simpler models [e.g., (25a) and (25b)]. Accordingly, the same numerical techniques can be used to solve both type of models. Thus, CMO is computationally as efficient as any classical bulk model, though it handles more complex physics.

b. *The behavior of CMO in a nondimensional form*

Let us define the mixing efficiency

$$P^* = h\Delta b w_e / u_*^3. \tag{53}$$

In CMO, as in most classical models, the dimensionless parameter P^* is a function of h/L and h/λ only. The plots of $P^*(h/L, h/\lambda)$ are useful tools for comparing the different existing models (GAR). Such graphs for CMO and NK are displayed on Fig. 6. It appears that in unstable cases, the two models behave similarly. In stable situations, for increasing h/L, P^* decreases more slowly in CMO than in NK and reaches zero in an almost asymptotic manner, a behavior not simulated by other ML models. On the other hand, the mixing efficiency of CMO decreases with h/λ so that a value of h/λ exists for which $P^*(0, h/\lambda) = 0$. Garwood has shown that models having this property are able to simulate a cyclical steady state. Such is not the case for NK.

c. *The equilibrium depth in the neutral case*

In the neutral case, the equilibrium relation (52) can only be satisfied if $c_{p3} = 0$. Using (34) and (48), this condition yields

$$\frac{h}{\lambda} = c_\lambda = \frac{0.4}{a_2}\left[\frac{m_4(a_1 + a_2)(m_2 + m_3)}{m_2 + m_3 - m_5 m_3} - a_1\right]. \tag{54}$$

For the chosen values of the model constants (see appendix A), one obtains $c_\lambda = 2.9$. This value is consistent with the experimental results of Armi and Millard (1976) who deduce $c_\lambda = 2.4$ from observations of the benthic boundary layer.

It should also be mentioned that the condition $c_{p3} = 0$ would never have been verified if we had set $l_p = l$. The hypothesis through which l_p is allowed to be different from l is thus fundamental to obtain a neutral equilibrium depth in this type of model.

d. *The equilibrium depth in the stable case*

When the rotational constraint is not active, the equilibrium can only be reached in stable situations. The Eq. (52) then yields

$$h = c_e L \tag{55}$$

where $c_e = c_{p3}/c_{p1}$. This equilibrium relation is identical with that of NK (25b) with $c_e = 2m$. Using (27), NK yields $0.8 \leqslant c_e \leqslant 1$. From CMO we rather obtain $c_e = 4.5$. This relatively large value of c_e is a consequence of the slow decrease of the CMO mixing efficiency in stable conditions.

9. Testing GAR and CMO at *Weathership P*

a. *Numerical simulations with the GAR model*

As CMO uses the closure technique developed for the GAR model, it was useful to compare these two models. Garwood determines the ML depth from the basic set of equations (35), (43) and (49) with the following differences from CMO:

(i) h/l is given by (32) instead of (34). When the rotational constraint is neglected, (32) is a particular case of (34) for which $a_2 = 0$.

(ii) h/l_p is kept constant. This constant can be absorbed into the value of m_4.

(iii) only the return-to-isotropy term of Rotta (1951) is taken into account for the parameterization of the pressure-strain correlation term, i.e., $m_5 = 0$ in (49).

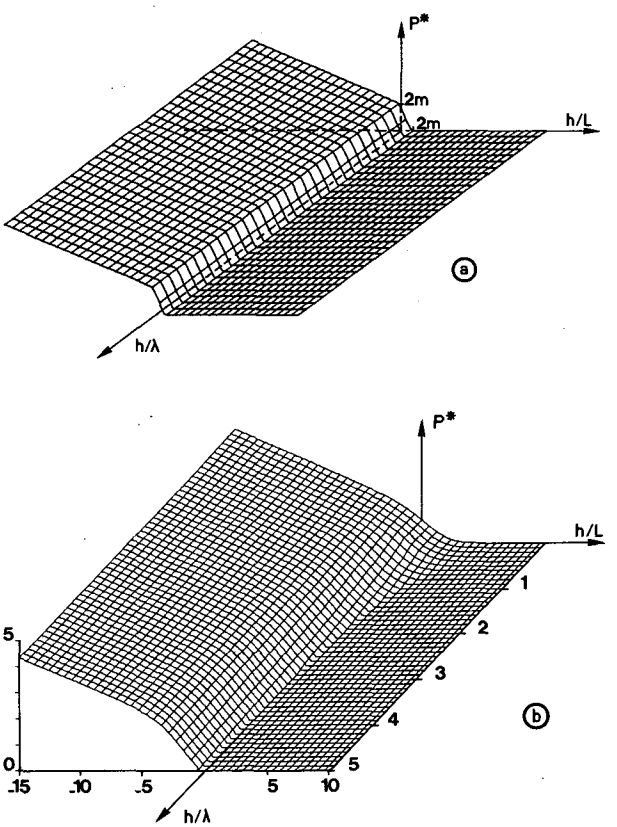

FIG. 6. The mixing efficiency P^* of (a) the NK and (b) CMO models as a function of the stability and rotation parameters.

Consequently, when the rotational effects are negligible, GAR is exactly a particular case of CMO for which a_1 is identical to k_1 and

$$m_5 = 0 \tag{56}$$

$$a_2 = 0. \tag{57}$$

However, replacing the calibration constraints (A1) and (A14) (see appendix A) by (56) and (57) respectively, it was not possible to obtain a set of constants for the GAR model that meets the other calibration constraints. Rather, we followed GAR and fixed $m_1 = k_1 = m_4/3 = 1$ while $m_2 + m_3$ and k_2 were left to be adjusted. Using $m_2 + m_3 = 4.5$ and $k_2 = 4.6$, Martin (1985) obtained errors on the monthly mean SST simulated by the GAR model nearly reaching 2 K at Station P. After some calibration experiments, we obtained better results with $m_2 + m_3 = 3.4$ and $k_2 = 0.8$. It should be remarked that, in the neutral case when the rotational effects are negligible, the mixing efficiency of the GAR model is given by

$$P^* = \frac{m_2 + m_3}{(2m_4/m_1^2) - (2 + m_4)/6} \times \left[\left(\frac{1}{4} + \frac{4m_4(m_4 - 1)}{3m_1^2}\right)^{1/2} - \frac{1 + 2m_4}{6}\right]. \tag{58}$$

Always in the neutral case, the GAR model stops entraining for

$$\frac{h}{\lambda} = c_\lambda = \frac{m_4 - k_1}{k_2}\left(\frac{m_2 + m_3}{m_4}\right)^{1/3}. \tag{59}$$

Using the Martin (1985) calibration, (58) and (59) yield $P^* = 1.5$ and $c_\lambda = 0.5$, respectively. With the present calibration, one obtains, $P^* = 1.1$ and $c_\lambda = 2.6$. These values are closer to those observed by Davis et al. (1981) ($0.8 \leq P^* \leq 1$) and Armi and Millard (1976) ($c_\lambda = 2.4$).

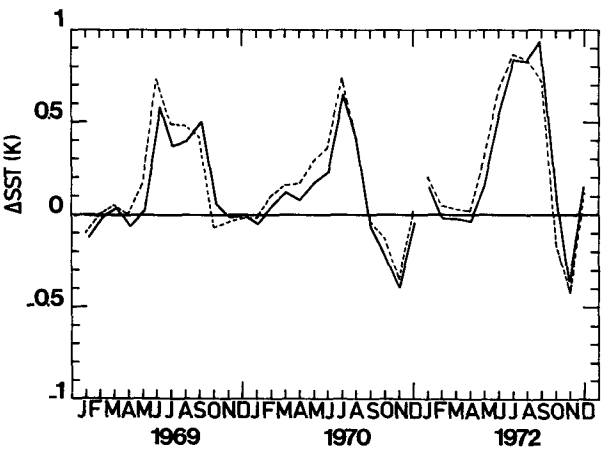

FIG. 7. ΔSST for the GAR model (solid curve) compared to ΔSST for the Wells model (dashed curve). Station P, years 1969, 1970 and 1972.

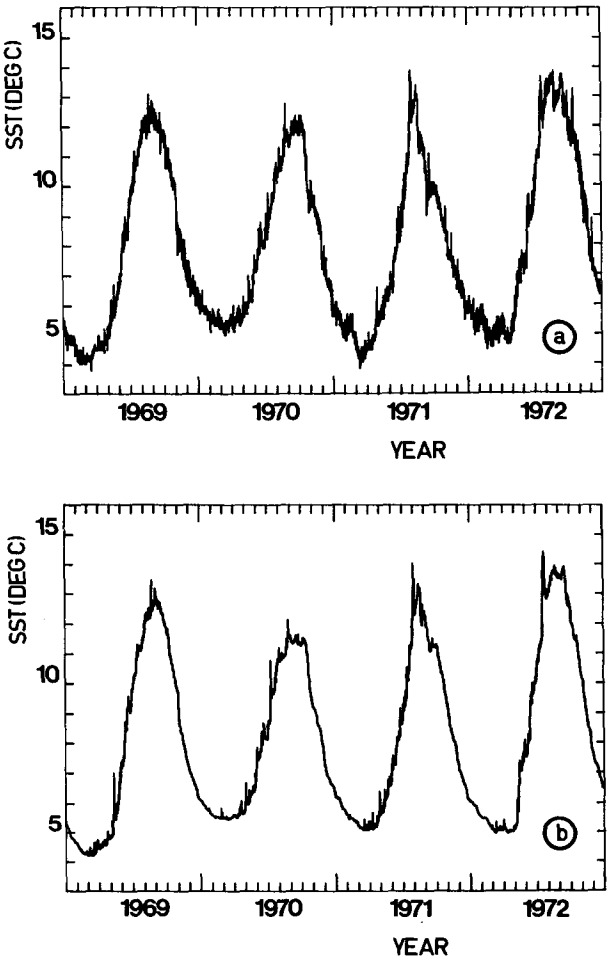

FIG. 8. (a) Observed and (b) CMO simulated 3-hourly SST at station P during the years 1969 to 1972.

A 4-year simulation at Station P was performed with the so-calibrated GAR model. In the absence of a single entrainment equation like (50), E_m and W_m were determined at each time step to compute the ML depth variations. The model had the same vertical resolution, time step, initialization and surface fluxes as those used for the NK model. The monthly mean predicted SST exhibited errors larger than 1 K only during March and September 1971. The same errors were already observed and discussed in the NK simulations. For the three other years, the model's performances are similar to those of the Wells model (Fig. 7). The autumn error is reduced, in comparison with NK, but the summer error persists with the same amplitude.

b. Numerical simulations with CMO

Using again the same numerical characteristics, a 4-year simulation at station P was performed using CMO. As seen on Fig. 8, it does fairly well in reproducing the seasonal and interannual variations of the SST. As in

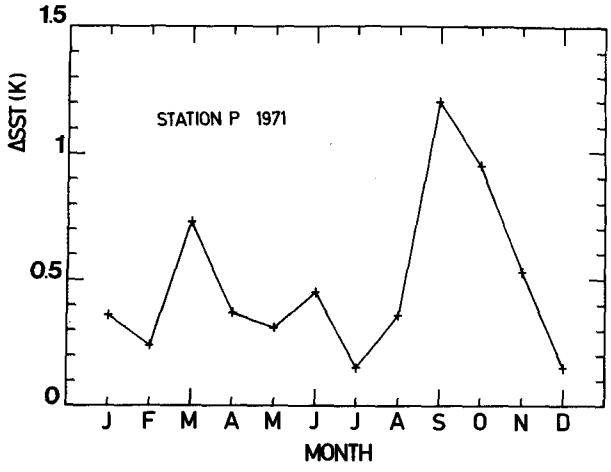

FIG. 9. ΔSST for the CMO model. Station P, year 1971.

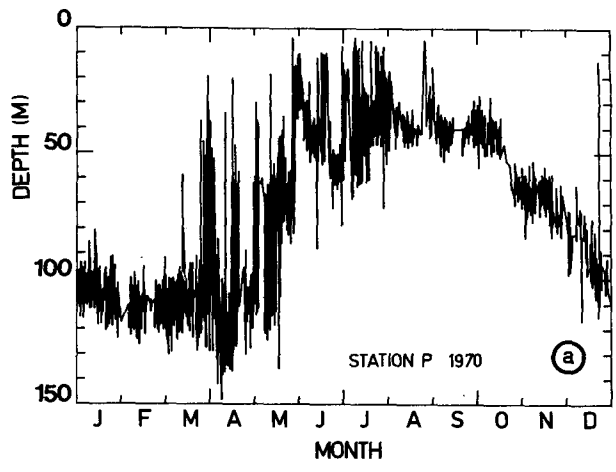

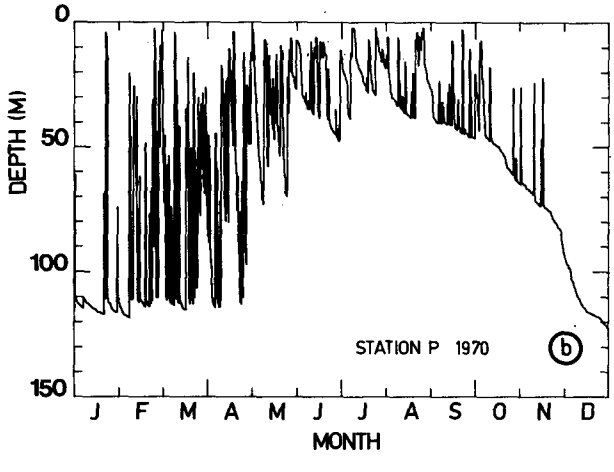

FIG. 11. (a) Observed and (b) CMO simulated 3-hourly ML depth at station P during the year 1970.

the previous simulations, large errors appear only in March and September of 1971 (Fig. 9). For the other three years, the difference between the simulated and observed monthly mean SST (ΔSST) remains smaller than 0.5 K (Fig. 10). Compared with Wells or GAR, CMO mainly conduces to a reduction of the summer error. Yet, the annual evolution of SST is analogous to that observed with the other models; the SST tends to be overestimated in summer and underestimated in autumn. Accordingly, the simulated ML depths are too small in summer and increase too rapidly in autumn (see the example on Fig. 11).

Additional 4-year simulations were performed to examine the sensitivity of CMO to the chosen calibration. Using successively the minimal and maximal permitted values of m_1 (0.37 and 0.52, see appendix A), we obtained two extreme sets of constants with the method of calibration described in appendix A. On a monthly mean, and for any of these two calibrations, the simulated SST never differs by more than 0.1 K from that obtained with the standard calibration.

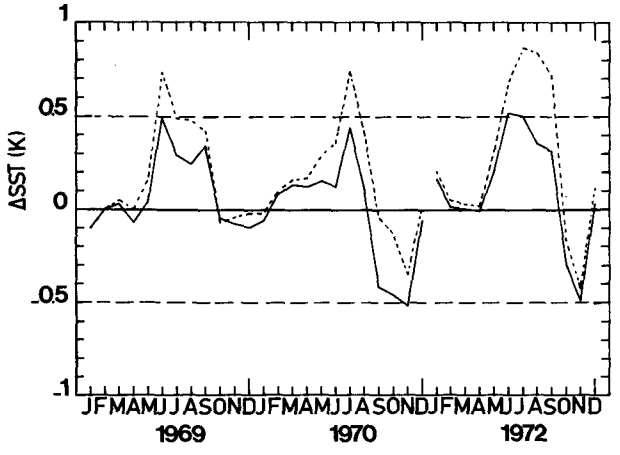

FIG. 10. ΔSST for the CMO model (solid curve) compared to ΔSST for the Wells model (m_w = 0.8; dashed curve). Station P, years 1969, 1970 and 1972.

It should be pointed out that the use of a high vertical resolution is not critical for the model results. To assess this, a simulation was performed with a resolution reduced to ten levels (at 5, 10, 15, 20, 30, 40, 50, 75, 100 and 150 m). This caused a maximum change of 0.1 K in the simulated monthly mean SST as compared to the standard simulation. The sensitivity of CMO to the chosen time step was also tested. A 3-hour time step was used in the presented simulations as it corresponded to the sampling period of the surface forcing. It roughly resolves the diurnal cycle. The use of shorter time steps did not induce significant changes of the results. For example, a four-year simulation was performed using a time step of 30 minutes. In comparison with the standard simulation, a maximum change of 0.12 K was obtained for the simulated monthly mean SST.

c. The persistent error

1) SUMMER ERROR

In all models studied, the summer overestimation of the SST reaches its maximum in June or July when the heat gain from the surface is also maximum. During this period, the stable situations often causing a ML retreat are prevailing. The simulation results are thus critically dependent on the model behavior in these stable situations and on the predicted equilibrium depth. As previously noticed, when the stability increases, the mixing efficiency of CMO decreases more slowly than in the models of the NK type. It also decreases more slowly than in the GAR model (Fig. 12). With the here-used calibrations, the models of the NK type reach equilibrium for values of h/L between 1.3 and 1.6, when the rotational constraint is negligible. Under the same condition, the GAR model yields an equilibrium value of $h/L = 2.7$, while CMO maintains entrainment up to $h/L = 4.5$. The CMO thus favors entrainment in stable cases and predicts larger equilibrium depths than the other models. Therefore, CMO tends to simulate deeper summer MLs, in better agreement with observations. The simulation of the SST is accordingly improved though a slight overestimation remains. These results tend to support those of Martin (1985) who noticed that the accuracy of NK is enhanced by an ad hoc increase of the constant m when used to predict the retreat depth.

Any further analysis of the persistent summer error is strongly limited by the poor existing knowledge on the behavior of the stable MLs. Until now, only a few experimental studies (e.g., Thorpe, 1978) have focused on the physics of stabilized MLs. Most observations have been for actively entraining layers. In fact, the retreat depth has little, if any, immediate signature on the vertical temperature profile, the most readily available data. This lack of data precludes a direct evaluation of the different expressions of the retreat depth used in the bulk models. Most of these expressions yield a depth that only depends on L and/or λ. However, it could be that the depth of the zone of wave influence (typically six to ten times the wave height) is an additional pertinent length, especially during summer periods when it is not negligible compared with h. This still has to be investigated.

2) AUTUMN ERROR

All studied models in which the rotational effect is parameterized, yield a reduced autumn error as compared to the basic NK model. Most of the remaining error should be due to a still insufficient parameterization of this effect. Further work on it could lead to improvement. Little guidance in this field is to be expected from the more sophisticated turbulence closure models. Indeed, most of them neglect the Coriolis term in the turbulent stresses equations though Mellor and Yamada (1982) point out that this issue deserves to be more thoroughly investigated. Some works of interest have been performed on simpler models by Svensson (1981) and Garwood et al. (1985), but these need to be generalized before they can be tested on annual simulations.

On the other hand, it should be noticed that Station P is not the ideal place to test parameterizations of Coriolis effects. Indeed, the sharp permanent halocline existing between 100 and 150 m, does not allow deep mixing. Consequently, the interval of possible values for the rotation parameter h/λ is strongly reduced. Other studies in oceanic regions where the ML reaches considerably larger depths are thus clearly desirable.

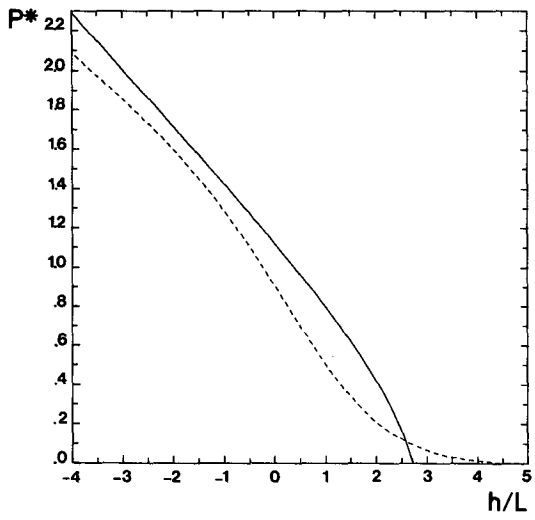

FIG. 12. The mixing efficiency P^* of the GAR (solid curve) and CMO (dashed curve) models as a function of the stability parameter h/L, when the rotational effects are neglected ($h/\lambda = 0$).

10. Summary and conclusion

Focusing on the long-term response, the parameterization of the turbulence used in one-dimensional models of the ML was rapidly reviewed. Particular attention was paid to a weak point, the parameterization of the turbulent dissipation rate. A general formulation was proposed that provides a useful guideline to devise new parameterizations and compare the existing ones.

Several models were then tested by simulating the upper ocean at Station P during the years 1969 to 1972. A version of the now-classical NK model was first examined. After empirical calibration of the wind-mixing efficiency coefficient, a systematic simulation error persisted. The SST was overestimated in summer (h underestimated) and underestimated in autumn (h overestimated). On a monthly mean, the error in the predicted SST reached about 1 K in summer and -1 K in autumn. In addition, an important error appeared in September 1971 in conjunction with a sudden change in the thermocline stratification. This event

could not be simulated by the simple thermodynamic model used for the thermocline. The error persisted for several months, until the thermocline was completely eroded.

Runs were also performed with the Resnyanskiy (1975) and Wells (1979) models in which a rotational constraint acts on the parameterized turbulent dissipation. This constraint proved to be useful in limiting the autumnal erosion of the thermocline. The error in the predicted autumnal SST was accordingly reduced by a few tenths of a degree. Nevertheless, after tuning, these models retained a systematic error similar to that of NK.

In an attempt to cope with these problems, a new model (CMO) was proposed for the prediction of the ML depth. It consists of a set of three equations with three unknowns (h, E_m, W_m) and uses the Garwood (1977) bulk closure technique.

(i) The first equation is the classical TKE budget of the ML in which a new parameterization of the dissipation is used; $E_m^{1/2}$ is introduced as the characteristic turbulent velocity instead of the more usual u_*. Explicit use can therefore be made of a novel dissipation length that is stability and rotation dependent;

(ii) The second equation is a parameterized form of the TKE balance at the base of the ML. Its deduction is based on an analysis of the results of high-order turbulence closure models. This analysis shows that entrainment is mainly controlled by the downward turbulent transfer of TKE and momentum. The parameterization of this mechanism finally leads to the GAR entrainment equation that was originally obtained using different arguments;

(iii) An equation for W_m is obtained by parameterizing the depth-integrated equation for $\overline{w'^2}$. Use is made of the Launder's (1975) parameterization of the pressure-strain correlation term.

The CMO was calibrated using several measurements of turbulent flows, and a result of the André and Lacarrère (1985) third-order turbulence closure model. An examination of the CMO set of equations revealed that the evolution of h can be predicted from a single equation from which E_m and W_m have been eliminated. Consequently, although handling the ML physics more rigorously, CMO is numerically as efficient as the previously considered models.

The original Garwood (1977) model was then tested on a 4-year simulation at station P. Its results were similar to those of the Resniyanskiy (1975) or Wells (1979) models. The same 4-year simulation was finally performed using CMO. This model succeeded in predicting the SST with a monthly-mean error less than 0.5 K. Yet, the summer SST still tends to be overestimated (h underestimated) and the autumn SST underestimated (h overestimated).

Compared with the previously studied models, CMO mainly yields a reduced summer error because of the unique behavior of its mixing efficiency in stable situations. A further examination of the remaining error is strongly limited by the poor existing knowledge on stable MLs. In order to progress, more observations of stabilized or retreating layers should be made. As the retrieval of the ML depth from the usual BT data is often problematical, especially in stable cases, one should intensify the acquisition of turbulent dissipation profiles. From these profiles, a precise determination of h, identified as the turbocline depth, is possible (Woods and Barkmann, 1986). It is also suggested that the zone of surface wave influence should be more particularly investigated as it often occupies a large portion of the shallow summer MLs.

The persistent autumn error probably indicates an insufficient parameterization of the rotational effects. Again, little information is available at present on this topic. Furthermore, station P is not the ideal place to test parameterizations of the Coriolis effects. It is thus desirable that such tests be repeated for oceanic regions where deep winter mixing is known to occur.

Acknowledgments. Special thanks go to A. Berger for continued support and encouragement. Thanks are extended to J. C. André, J. Nihoul, R. Pollard, N. Wells and J. Woods for many stimulating discussions, comments and suggestions. Ch. Tricot kindly supplied the surface fluxes and P. Lacarrère supplied calibration data. The meteorological and oceanographic data from Station P were provided by the Canadian Marine Environmental Data Service. The advice of F. Dobson and S. Tabata was of valuable assistance for the processing of these data. The author is supported by the National Fund for Scientific Research (Belgium) and the Commission of the European Communities under Contract ST2A-0010-2-F (CD). This support is gratefully acknowledged. This paper was written while the author was visiting the Centre National de Recherches Météorologiques (Toulouse, France).

APPENDIX A

The Calibration of CMO

1. The calibration scheme

On the basis of a Crow's (1968) result, Launder (1975) deduced:

$$m_5 = 0.6. \tag{A1}$$

Using the results of several experiments on convective or neutral shear flows listed in section 2, the following dimensionless ratios can be determined.

(i) For purely convective flows

$$W_m/E_m = i_1; \quad W_m/w_*^2 = i_2; \quad -h\overline{b'w'}(-h)/w_*^3 = i_3 \tag{A2}$$

where $w_* = [-hB(h)]^{1/3}$, the Deardorff (1970) convective velocity scale.

(ii) For neutral shear flows

$$W_m/E_m = n_1; \quad E_m/u_*^2 = n_2; \quad -h\overline{b'w'}(-h)/u_*^3 = n_3. \tag{A3}$$

In convective cases, the definitions of the characteristic lengths (34) and (48) reduce to

$$h/l = h/l_p = a_1. \tag{A4}$$

In the neutral flow experiments used for calibration the rotational constraint was not active ($h < 0.4\lambda$) so that

$$h/l = h/l_p = a_1 + a_2. \tag{A5}$$

For convective flows, the introduction of (A2) and (A4) into the model equations (35), (43) and (49) yields, successively

$$a_1 = 0.5(1 - i_3)(i_1/i_2)^{3/2} \tag{A6}$$

$$m_1 = i_1 i_3 i_2^{-3/2} \tag{A7}$$

and after some algebra

$$(1 - m_5)/m_4 = 0.5(3i_1 - 1). \tag{A8}$$

Similarly, for neutral flows, the introduction of (A3) and (A5) into (35), (43) and (49) yields

$$m_2 + m_3 - (a_1 + a_2)n_2^{3/2} = 0.5n_3 \tag{A9}$$

$$m_1 = n_3 n_2^{-3/2} n_1^{-1/2} \tag{A10}$$

$$m_5 m_3 + [m_4(1 - 3n_1) - 1](a_1 + a_2)n_2^{3/2} = (1.5 - m_5)n_3. \tag{A11}$$

Equation (A6) directly determines a_1 and the value of m_4 is obtained from (A1) and (A8). Equations (A7) and (A10) both provide a determination of m_1. The two remaining relations (A9) and (A11) are not sufficient to determine the three constants still unknown: m_2, m_3 and a_2. Use is therefore made of the third-order turbulence closure model of André and Lacarrère (1985). Depth-integrated results of several simulations performed with this model indicate that the ratio:

$$n_4 = \frac{(h\epsilon_m/E_m^{3/2})_{\text{neutral flow}}}{(h\epsilon_m/E_m^{3/2})_{\text{convective flow}}} \tag{A12}$$

remains almost exactly constant, its value being (Lacarrère, 1983, personal communication):

$$n_4 = 1.5. \tag{A13}$$

With the parameterization of $h\epsilon_m$ used in CMO, (A12) and (A13) reduce to

$$(a_1 + a_2)/a_1 = 1.5. \tag{A14}$$

This completes the calibration scheme.

2. Calibration data

By definition, i_3 and n_3 are respectively identical to the constants n and $2m$ of the NK model. Accordingly, (26) and (27) immediately yield

TABLE 3. Estimates of the dimensionless parameters i_1 and i_2 defined in Eq. (A2).

Author	i_1	i_2	Source
Willis and Deardorff (1974)	S1 0.45 S2 0.44	0.33 0.38	Laboratory experiments in a convection chamber. Two experiments (S1 and S2) were performed with different initial stratifications.
Frangi (1979)		0.38	Collection of data from various French experiments on the atmospheric convective boundary layer.
Lenschow et al. (1980)		0.31	Data from AMTEX (observation of the atmospheric convective boundary layer).

$$i_3 = 0.2 \tag{A15}$$

$$0.8 \leqslant n_3 \leqslant 1. \tag{A16}$$

Estimates of i_1 and i_2 are obtained from vertically integrated results of different experiments listed in Table 3. These give

$$0.44 \leqslant i_1 \leqslant 0.45 \tag{A17}$$

$$0.31 \leqslant i_2 \leqslant 0.38. \tag{A18}$$

Concerning neutral boundary layers, n_1 and n_2 are estimated from integrated results of the widely quoted Klebanoff (1955) experiment. It should be pointed out that the outer edge of a neutral boundary layer is always less sharply defined than that of a convective layer. Given that uncertainty on the boundary layer thickness, one obtains

$$0.18 \leqslant n_1 \leqslant 0.2 \tag{A19}$$

$$2.6 \leqslant n_2 \leqslant 3. \tag{A20}$$

3. Numerical calibration

Introducing (A15), (A17), (A18) into (A7) and (A16), (A19), (A20) into (A10), one obtains for a convective boundary layer

$$0.37 \leqslant m_1 \leqslant 0.52 \tag{A21}$$

and for a neutral boundary layer

$$0.35 \leqslant m_1 \leqslant 0.56. \tag{A22}$$

These two concordant estimations confirm that m_2 can effectively be considered as a constant for which one takes the intermediate value

$$m_1 = 0.45. \tag{A23}$$

For consistency, the values of $(i_1, i_2, i_3, n_1, n_2, n_3)$ have to be chosen, within the acceptable range, in such a way that both determinations of m_1 (A7 and A10) exactly verify (A23). The constant characterizing the

wind-mixing efficiency being fixed at its mean value, $n_3 = 0.9$, a consistent choice is

$$i_1 = 0.45, \quad i_2 = 0.34, \quad i_3 = 0.2$$
$$n_1 = 0.2, \quad n_2 = 2.7, \quad n_3 = 0.9. \qquad \text{(A24)}$$

The introduction of these numerical values into the previously described calibration scheme yields the final set of constants:

$$m_1 = 0.45, \ m_2 = 2.6, \ m_3 = 1.9, \ m_4 = 2.3,$$
$$m_5 = 0.6, \quad a_1 = 0.6, \quad a_2 = 0.3. \qquad \text{(A25)}$$

APPENDIX B

A Method of Solution for CMO

For the reader's ease, the three model equations (35), (43) and (49) are duplicated and identified with a number peculiar to this appendix:

$$0.5h\Delta bw_e = (m_2 + m_3)u_*^3 - 0.5hB(h) - (h/l)E_m^{3/2} \qquad \text{(B1)}$$

$$h\Delta bw_e = m_1 E_m W_m^{1/2} \qquad \text{(B2)}$$

$$(0.5 - m_5/3)[h\Delta bw_e + hB(h)] = [(m_4 h/3l_p) - (h/3l)]E_m^{3/2} + (m_5 m_3/3)u_*^3 - (m_4 h/l_p)E_m^{1/2}W_m. \qquad \text{(B3)}$$

1. Entrainment condition

For entrainment to occur, w_e has to be strictly positive, Equation (B1) shows that a necessary condition for this is

$$S_p = (m_2 + m_3)u_*^3 - 0.5hB(h) > 0. \qquad \text{(B4)}$$

This simply means that entrainment is only possible when the total supply of TKE to the ML (S_p) is positive. By definition, E_m is larger than W_m and consequently it appears from (B2) that a necessary and sufficient condition for entrainment to occur is

$$W_m > 0. \qquad \text{(B5)}$$

Eliminating $h\Delta bw_e$ between (B1) and (B3), one obtains

$$W_m = (2c_{p1}/m_4)E_m - (c_2 l_p/m_4 h)u_*^3 E_m^{-1/2} \qquad \text{(B6)}$$

where W_m is expressed as a function of E_m. For the chosen values of the model coefficients (A25), c_2 is a positive constant:

$$c_2 = [(3 - 2m_5)(m_2 + m_3) - m_5 m_3]/3$$

and c_{p1} is a positive function of l_p/l

$$c_{p1} = [(2 - 2m_5)(l_p/l) + m_4]/6.$$

Thus W_m is a strictly increasing function of E_m and there is a single value of E_m for which W_m becomes zero:

$$E_{m0} = (c_2 l_p/2c_{p1}h)^{2/3}u_*^2. \qquad \text{(B7)}$$

It follows that the entrainment condition (B5) is equivalent to

$$E_m > E_{m0}. \qquad \text{(B8)}$$

This indicates that entrainment only occurs if the TKE exceeds a minimum level given by (B7). Eliminating $h\Delta bw_e$ between (B1) and (B2), the value of E_m is found as the root of the function

$$F(E_m) = 0.5m_1 E_m W_m^{1/2} + (h/l)E_m^{3/2} - S_p$$

in which W_m can be expressed as a function of E_m due to (B6). For $E_m > E_{m0}$, F is a strictly increasing function of E_m. Consequently, (B8) can be satisfied, i.e., entrainment can occur, if and only if

$$F(E_{m0}) < 0 \qquad \text{(B9)}$$

or equivalently if

$$A_p = S_p - (h/l)E_{m0}^{3/2} > 0. \qquad \text{(B10)}$$

This means that entrainment only occurs if S_p, the total supply of TKE, is greater than the minimal dissipation (i.e., the dissipation associated with E_{m0}, the minimal possible value of E_m during entrainment); A_p is thus the maximal amount of turbulent energy available for entrainment.

The value of E_{m0} being given by (B7), the necessary and sufficient entrainment condition (B10) can be explicitly rewritten:

$$A_p = c_{p3}u_*^3 - c_{p1}hB(h) > 0 \qquad \text{(B11)}$$

with

$$c_{p3} = [m_4(m_2 + m_3) - (l_p/l)(m_2 + m_3 - m_5 m_3)]/3.$$

Due to this relation, the decision for entrainment or retreat in the numerical implementation of CMO is made as simple as in any model of the NK type.

2. Retreat

In the cases where (B11) cannot be satisfied, it is assumed that h automatically adjusts so as to maintain

$$A_p = 0. \qquad \text{(B12)}$$

When $B(h)$ is nonzero, this is equivalent to

$$h = (c_{p3}/c_{p1})L. \qquad \text{(B13)}$$

This equation for the equilibrium depth is analogous to that used in the NK model (25b). Notice, however, that c_{p3}/c_{p1} is not a constant but a function of both h/L and h/λ.

3. A single equation for the entrainment velocity

In order to obtain a single equation governing the evolution of the ML depth, E_m and W_m have to be eliminated from the set of equations (B1) to (B3). To facilitate the writing, let us set

$$h\Delta bw_e = X.$$

Equation (B2) can be rewritten so as to give E_m as a function of X:

$$E_m = (h/l)^{-2/3}(S_p - 0.5X)^{2/3}. \quad \text{(B14)}$$

Also W_m can be obtained as a function of X by introducing (B14) into (B6). This yields

$$W_m = (A_p - c_{p1}X)[m_4(S_p - 0.5X)^{1/3}(h/l)^{2/3}]^{-1}. \quad \text{(B15)}$$

Finally, using (B14) and (B15) to eliminate E_m and W_m from (B2), one obtains, after some algebra

$$[m_4(h/m_1l)^2 - 0.5c_{p1}]X^2 + (0.5A_p + c_{p1}S_p)X - S_pA_p = 0. \quad \text{(B16)}$$

The coefficient of X^2 is always positive and the entrainment conditions (B4) and (B10) imply $0.5A_p + c_{p1}S_p > 0$ and $S_pA_p > 0$. It follows that the quadratic equation (B16) has two real roots of opposite sign. Only the positive one has a physical meaning. It takes the form:

$$h\Delta bw_e = \frac{-(0.5A_p + c_{p1}S_p) + [(0.5A_p - c_{p1}S_p)^2 + 2c_4(h/l)^2A_pS_p]^{1/2}}{c_4(h/l)^2 - c_{p1}} \quad \text{(B17)}$$

where

$$c_4 = 2m_4m_1^{-2}. \quad \text{(B18)}$$

So, the entrainment term (X) is explicitly obtained as a nonlinear function of S_p, the mechanical plus buoyant supply of TKE, and A_p, the maximal amount of TKE available for entrainment.

REFERENCES

Adamec, D., R. L. Elsberry, R. W. Garwood and R. L. Haney, 1981: An embedded mixed-layer-ocean circulation model. *Dyn. Atmos. Oceans*, **6**, 69–96.

Alexander, R. C., and J. W. Kim, 1976: Diagnostic model study of mixed layer depths in the summer North Pacific. *J. Phys. Oceanogr.*, **6**, 293–298.

André, J. C., G. De Moor, P. Lacarrère, G. Therry and R. du Vachat, 1978: Modelling the 24-hour evolution of the mean and turbulent structures of the planetary boundary layer. *J. Atmos. Sci.*, **35**, 1861–1883.

——, and P. Lacarrère, 1985: Mean and turbulent structures of the oceanic surface layer as determined from one-dimensional, third order simulations. *J. Phys. Oceanogr.*, **15**, 121–132.

Armi, L., and R. C. Millard, 1976: The bottom boundary layer of the deep ocean. *J. Geophys. Res.*, **81**, 4983–4990.

Artaz, M. A., and J. C. André, 1980: Similarity studies of entrainment in convective mixed layers. *Bound.-Layer Meteor.*, **19**, 51–66.

Ball, F. K., 1960: Control of inversion height by surface heating. *Quart. J. Roy. Meteor. Soc.*, **86**, 483–494.

Boers, R., E. W. Eloranta and R. L. Coulter, 1984: Lidar observations of mixed layer dynamics: tests of parameterized entrainment models of mixed layer growth rate. *J. Climate. Appl. Meteor.*, **23**, 247–266.

Bryan, K., and M. D. Cox, 1972: An approximate equation of state for numerical models of ocean circulation. *J. Phys. Oceanogr.*, **2**, 510–514.

Bunker, A. F., 1976: Computations of surface energy flux and annual air-sea interaction cycle of the North Atlantic Ocean. *Mon. Wea. Rev.*, **104**, 1122–1140.

Caughey, S. J., 1982: Observed characteristics of the atmospheric boundary layer. *Atmospheric Turbulence and Air Pollution Modelling*, F. T. M. Nieuwstadt and H. van Dop, Eds., Reidel, 107–158.

Crow, S. C., 1968: Viscoelastic properties of fine-grained incompressible turbulence. *J. Fluid Mech.*, **33**, 1–20.

Davis, R. E., R. de Szoeke, D. Halpern and P. Niiler, 1981a: Variability in the upper ocean during MILE. Part I: The heat and momentum balances. *Deep-Sea Res.*, **28A**, 1427–1451.

——, —— and P. P. Niiler, 1981b: Variability in the upper ocean during MILE. Part II: Modelling the mixed layer response. *Deep-Sea Res.*, **28A**, 1453–1475.

Deardorff, J. W., 1970: Convective velocity and temperature scales for the unstable planetary boundary layer and for Rayleigh convection. *J. Atmos. Sci.*, **27**, 1211–1213.

——, 1980: Comments on "A numerical investigation of mixed layer dynamics". *J. Phys. Oceanogr.*, **10**, 1695–1696.

——, 1983: A multi-limit mixed-layer entrainment formulation. *J. Phys. Oceanogr.*, **13**, 988–1002.

——, and S. C. Yoon, 1984: On the use of an annulus to study mixed-layer entrainment. *J. Fluid Mech.*, **142**, 97–120.

Dillon, T. M., J. G. Richman, C. G. Hansen and M. D. Pearson, 1981: Near-surface turbulence measurements in a lake. *Nature*, **290**, 390–392.

Dobson, F. W., F. P. Bretherton, D. M. Burridge, J. Crease, E. B. Kraus and T. H. Vonder Haar, 1982: The CAGE experiment. A feasibility study. Rep. WCP-22. World Meteorological Organization, 95 pp.

Driedonks, A. G. M., 1982: Models and observations of the growth of the atmospheric boundary layer. *Bound.-Layer Meteor.*, **23**, 283–306.

Elsberry, R. L., T. S. Fraim and R. N. Trapnell, 1976: A mixed layer model of the oceanic thermal response to hurricanes. *J. Geophys. Res.*, **81**, 1153–1162.

——, and R. W. Garwood, 1980: Numerical ocean prediction models. Goal for the 1980s. *Bull. Amer. Meteor. Soc.*, **61**, 1556–1566.

Farmer, D. V., 1975: Penetrative convection in the absence of mean shear. *Quart. J. Roy. Meteor. Soc.*, **101**, 869–891.

Frangi, J. P., 1979: Contribution à l'étude de la structure verticale des principales caractéristiques de la couche limite planétaire. Thèse de 3ème cycle. Université de Paris VII, 129 pp.

Friehe, C. A., and K. F. Schmitt, 1976: Parameterization of air-sea interface fluxes of sensible heat and moisture by the bulk aerodynamic formulas. *J. Phys. Oceanogr.*, **6**, 801–809.

Gargett, A. E., T. B. Sanford and T. R. Osborn, 1979: Surface mixing layers in the Sargasso Sea. *J. Phys. Oceanogr.*, **9**, 1090–1111.

Garnich, N. G., and S. A. Kitaigorodskii, 1977: On the rate of deepening of the oceanic mixed layer. *Izv. Atmos. Ocean. Phys.*, **13**, 888–893.

Garrett, C., 1979: Mixing in the ocean interior. *Dyn. Atmos. Oceans*, **3**, 239–265.

Garwood, R. W., 1977: An oceanic mixed layer model capable of simulating cyclic states. *J. Phys. Oceanogr.*, **7**, 455–468.

——, and J.-Y. Yun, 1979: Bulk closure for the oceanic planetary boundary layer. *Proc. Second Symp. on Turbulent Shear Flows*. Imperial College, London, 12.6–12.11.

——, P. C. Gallacher and P. Muller, 1985: Wind direction and equilibrium mixed layer depth: general theory. *J. Phys. Oceanogr.*, **15**, 1325–1331.

Gaspar, Ph., 1985a: An oceanic mixed layer model suitable for climatological studies: Results over several years of simulation. *The Ocean Surface*, Y. Toba and H. Mitsuyasu, Eds., D. Reidel, 509–516.

——, 1985b: Modèles de la couche active de l'océan pour des simulations climatiques. Ph.D. thesis, Université Catholique de Louvain-La-Neuve, Belgium. 187 pp.

Heidt, F. D., 1977: The growth of the mixed layer in a stratified fluid due to penetrative convection. *Bound.-Layer Meteor.*, **12**, 439–461.

Jerlov, N. G., 1976: *Marine Optics. Elsevier Oceanogr. Ser.*, Vol. 14, 231 pp.

Kim, J. W., 1976: A generalized bulk model of the oceanic mixed layer. *J. Phys. Oceanogr.*, **6**, 686–695.

Kitaigorodskii, S. A., 1981: On the theory of the surface stress induced entrainment at a buoyancy interface. *Tellus,* **33,** 89–101.

——, M. A. Donelan, J. L. Lumley and E. A. Terray, 1983: Wave–turbulence interactions in the upper-ocean. Part II: Statistical characteristics of wave and turbulent components of the random velocity field in the marine surface layer. *J. Phys. Oceanogr.,* **13,** 1988–1999.

Klebanoff, P. S., 1955: Characteristics of turbulence in a boundary layer with zero pressure gradient, Rep. 1247, N.A.C.A. 19 pp.

Klein, P., 1979: Modélisation des mécanismes turbulents dans les couches marines superficielles (couche mélangée et thermocline). Thèse de Doctorat d'Etat. Université de Aix-Marseille II, 166 pp.

——, 1980: A simulation of the effects of air-sea transfer variability on the structure of marine upper layers. *J. Phys. Oceanogr.,* **10,** 1824–1841.

——, and M. Coantic, 1981: A numerical study of turbulent processes in the marine upper layers. *J. Phys. Oceanogr.,* **11,** 849–863.

Kolmogorov, A. N., 1942: The equation of turbulent motion in an incompressible fluid. *Izv. Akad. Nauk. SSSR, Ser. Fiz.,* **6,** No. 1, 2, 56–58.

Kondo, J., 1975: Air-Sea bulk transfer coefficients in diabatic conditions. *Bound.-Layer Meteor.,* **9,** 91–112.

Kraus, E. B., and J. S. Turner, 1967: A one-dimensional model of the seasonal thermocline. II. The general theory and its consequences. *Tellus,* **19,** 98–105.

Kundu, P. K., 1980a: A numerical investigation of mixed-layer dynamics. *J. Phys. Oceanogr.,* **10,** p. 1697.

——, 1980b: Reply to J. W. Deardorff's comments. *J. Phys. Oceanogr.,* **10,** 220–236.

Launder, B. E., 1975: On the effect of a gravitational field on the turbulent transport of heat and momentum. *J. Fluid Mech.,* **67,** 569–581.

Lenschow, D. H., J. C. Wyngaard and W. T. Pennell, 1980: Mean field and second moment budgets in a baroclinic, convective boundary layer. *J. Atmos. Sci.,* **37,** 1313–1326.

Lind, R. J., and K. B. Katsaros, 1982: A model of long wave irradiance for use with surface observations. *J. Appl. Meteor.,* **21,** 1015–1019.

Louis, J. F., A. Weill and D. Vidal-Madjar, 1983: Dissipation length in stable layers. *Bound.-Layer Meteor.,* **25,** 229–243.

Lumley, J. L., and B. Khajeh-Nouri, 1974: Computational modeling of turbulent transport. *Advances in Geophysics,* Vol. 18A, Academic Press, 169–192.

McPhaden, M. J., 1982: Variability in the central equatorial Indian Ocean. Part II: Oceanic heat and turbulent energy balances. *J. Mar. Res.,* **40,** 403–419.

Manabe, S., K. Bryan and M. J. Spelman, 1979: A global ocean–atmosphere climate model with seasonal variation for future studies of climate sensitivity. *Dyn. Atmos. Oceans,* **3,** 393–426.

Martin, P. J., 1985: Simulation of the mixed layer at OWS November and Papa with several models. *J. Geophys. Res.,* **90,** 903–916.

Mellor, G. L., and P. A. Durbin, 1975: The structure and dynamics of the ocean mixed layer. *J. Phys. Oceanogr.,* **5,** 718–728.

——, and T. Yamada, 1982: Development of a turbulence closure model for geophysical fluid problems. *Rev. Geophys. Space Phys.,* **20,** 851–875.

Miyakoda, K., and A. Rosati, 1984: The variation of sea surface temperature in 1976 and 1977. 2. The simulation with mixed layer models. *J. Geophys. Res.,* **89,** 6533–6542.

Moum, J. N., and D. R. Caldwell, 1985: Local influences on shear-flow turbulence in the equatorial ocean. *Science,* **230,** 315–316.

Niiler, P. P., 1975: Deepening of the wind-mixed layer. *J. Mar. Res.,* **33,** 405–422.

——, 1977: One-dimensional model of the seasonal thermocline. *The Sea,* Vol. VI, Wiley Interscience, 97–115.

——, and E. B. Kraus, 1977: One-dimensional models of the upper ocean. *Modelling and Prediction of the Upper Layers of the Ocean.* E. B. Kraus, Ed., Pergamon Press, 143–172.

Oakey, N. S., 1985: Statistics of mixing parameters in the upper ocean during JASIN phase 2. *J. Phys. Oceanogr.,* **15,** 1662–1675.

Paulson, C. A., and J. J. Simpson, 1977: Irradiance measurements in the upper ocean. *J. Phys. Oceanogr.,* **7,** 952–956.

Payne, R. E., 1972: Albedo of the sea surface. *J. Atmos. Sci.,* **29,** 959–970.

Pollard, R. T., P. B. Rhines and R. O. R. Y. Thompson, 1973: The deepening of the wind-mixed layer. *Geophys. Fluid Dyn.,* **3,** 381–404.

Price, J. F., R. A. Weller and R. Pinkel, 1986: Diurnal cycling: Observations and models of the upper ocean response to diurnal heating, cooling and wind mixing. *J. Geophys. Res.,* (Oceans), **91,** 8411–8427.

Resnyanskiy, Yu. D., 1975: Parameterization of the integral turbulent energy dissipation in the upper quasihomogeneous layer of the ocean. *Izv. Atmos. Ocean. Phys.,* **11,** 453–457.

Rotta, J. C., 1951: Statistische theorie nichthomogener turbulenz. *Z. Phys.,* **129,** 547–572.

Schopf, P. S., and M. A. Cane, 1983: On equatorial dynamics, mixed layer physics and sea surface temperature. *J. Phys. Oceanogr.,* **13,** 917–935.

Scranton, D. R., and W. R. Lindberg, 1983: An experimental study of entraining, stress-driven, stratified flow in an annulus. *Phys. Fluids,* **26,** 1198–1205.

Shay, J. J., and M. C. Gregg, 1984: Turbulence in an oceanic convective mixed layer. *Nature,* **310,** 282–285. [Corrigendum in *Nature,* **311,** 84.]

Smith, S. D., and F. W. Dobson, 1984: The heat budget at Ocean Weather Station Bravo. *Atmos.-Ocean.,* **22,** 1–22.

Stevenson, J. W., 1979: On the effect of dissipation on seasonal thermocline models. *J. Phys. Oceanogr.,* **9,** 57–64.

Stull, R. B., 1976: The energetics of entrainment across a density interface. *J. Atmos. Sci.,* **33,** 1260–1267.

Svensson, U., 1981: On the influence of buoyancy on the turbulent Ekman layer. *Proc. Third Symp. on Turbulent Shear Flows.* University California, 12.5–12.11.

Tabata, S., 1964: A study of the main physical factors governing the oceanographic conditions at Ocean Station "P" in the Northeast Pacific Ocean. Ph.D. thesis, University of Tokyo, 264 pp.

Therry, G., and P. Lacarrère, 1983: Improving the eddy kinetic energy model for planetary boundary layer description. *Bound.-Layer Meteor.,* **25,** 63–88.

Thompson, R. O. R. Y., 1976: Climatological numerical models of the surface mixed layer of the ocean. *J. Phys. Oceanogr.,* **6,** 496–503.

Thorpe, S. A., 1978: The near-surface ocean mixing layer in stable heating conditions. *J. Geophys. Res.,* **83,** 2875–2885.

Tricot, Ch., 1985: Estimation des flux de chaleur en surface à la station météo-océanographique Papa. Sci. Rep. 1985/9, Institut d'Astronomie et de Géophysique G. Lemaître. Université Catholique de Louvain, Belgium.

Warn-Varnas, A. C., and S. A. Piacsek, 1979: An investigation of the importance of the third-order correlations and choice of length scale in mixed layer modelling. *Geophys. Astrophys. Fluid Dyn.,* **13,** 225–243.

——, G. M. Dawson and P. J. Martin, 1981: Forecast and studies of the oceanic mixed layer during the MILE experiment. *Geophys. Astrophys. Fluid Dyn.,* **17,** 63–85.

Wells, N. C., 1979: A coupled ocean-atmosphere experiment: The ocean response. *Quart. J. Roy. Meteor. Soc.,* **105,** 355–370.

Willis, G. E., and J. W. Deardorff, 1974: A laboratory model of the unstable planetary boundary layer. *J. Atmos. Sci.,* **31,** 1297–1307.

Woods, J. D., 1983: Climatology of the upper boundary layer of the ocean. WCRP Publ. Ser., Vol. II, 147–179.

——, and W. Barkmann, 1986: The response of the upper ocean to solar heating. I: The mixed layer. *Quart. J. Roy. Meteor. Soc.,* **112,** 1–27.

Wu, J., 1982: Wind-stress coefficients over sea surface from breeze to hurricane. *J. Geophys. Res.,* **87,** 9704–9706.

Zeman, O., and H. Tennekes, 1977: Parameterization of the turbulent energy budget at the top of the daytime atmospheric boundary layer. *J. Atmos. Sci.,* **34,** 111–123.

Zilitinkevich, S. S., D. V. Chalikov and Yu. D. Resnyanskiy, 1979: Modelling the oceanic upper layer. *Oceanol. Acta,* **2,** 219–240.